applied sciences

MDPI

Article

Investigating the Effect of Cross-Modeling in Landslide Susceptibility Mapping

Kamila Pawluszek-Filipiak *, Natalia Oreńczak † and Marta Pasternak †

Institute of Geodesy and Geoinformatics, Wroclaw University of Environmental and Life Sciences, 50-375 Wroclaw, Poland; 111832@student.upwr.edu.pl (N.O.); 111837@student.upwr.edu.pl (M.P.)

* Correspondence: kamila.pawluszek-filipiak@upwr.edu.pl

† These authors contribute equally to this paper.

Received: 20 August 2020; Accepted: 7 September 2020; Published: 11 September 2020

Featured Application: Landslide Susceptibility Mapping using landslide inventory generated for the surrounding area can be generally carried out. However, the low reliability of such susceptibility map was observed in areas of critical geological structures. Thus, this should be borne in mind, when performing such a modeling in complex geological regions.

Abstract: To mitigate the negative effects of landslide occurrence, there is a need for effective landslide susceptibility mapping (LSM). The fundamental source for LSM is landslide inventory. Unfortunately, there are still areas where landslide inventories are not generated due to financial or reachability constraints. Considering this led to the following research question: can we model landslide susceptibility in an area for which landslide inventory is not available but where such is available for surrounding areas? To answer this question, we performed cross-modeling by using various strategies for landslide susceptibility. Namely, landslide susceptibility was cross-modeled by using two adjacent regions ("Łososina" and "Gródek") separated by the Rożnów Lake and Dunajec River. Thus, 46% and 54% of the total detected landslides were used for the LSM in "Łososina" and "Gródek" model, respectively. Various topographical, geological, hydrological and environmental landslide-conditioning factors (LCFs) were created. These LCFs were generated on the basis of the Digital Elevation Model (DEM), Sentinel-2A data, a digitized geological and soil suitability map, precipitation, the road network and the Różnów lake shapefile. For LSM, we applied the Frequency Ratio (FR) and Landslide Susceptibility Index (LSI) methods. Five zones showing various landslide susceptibilities were generated via Natural Jenks. The Seed Cell Area Index (SCAI) and Relative Landslide Density Index were used for model validation. Even when the SCAI indicated extremely high values for "very low" susceptibility classes and very small values for "very high" susceptibility classes in the training and validation areas, the accuracy of the LSM in the validation areas was significantly lower. In the "Łososina" model, 90% and 57% of the landslides fell into the "high" and "very high" susceptibility zones in the training and validation areas, respectively. In the "Gródek" model, 86% and 46% of the landslides fell into the "high" and "very high" susceptibility zones in the training and validation areas, respectively. Moreover, the comparison between these two models was performed. Discrepancies between these two models exist in the areas of critical geological structures (thrust and fault proximity), and the reliability for such susceptibility zones can be low (2–3 susceptibility zone difference). However, such areas cover only 11% of the analyzed area; thus, we can conclude that in remaining regions (89%), LSM generated by the inventory for the surrounding area can be useful. Therefore, the low reliability of such a map in areas of critical geological structures should be borne in mind.

Keywords: landslide; landslide susceptibility modeling; landslide controlling factors; landslide inventory

1. Introduction

A landslide is the movement of earthen materials down a slope under the influence of gravity [1] and occurs when earthen material exceeds the shear strength (resistance to shearing) [2]. Landslide events can cause damage to buildings, infrastructure and property and endanger human life [3–5]. According to [6], landslides are in seventh place when it comes to the destruction of human life and property. It is estimated that the frequency of landslides is increasing. The main reasons for the larger landslide vulnerability are (1) climate change and more extreme weather conditions; (2) the overexploitation of natural resources and deforestation, (3) growing urbanization and unrestrained land use, (4) the increased use of traditionally non-populated mountainous regions for recreational and transportation purposes, pushing the borders further into hazardous terrain [6].

In Poland, the area most susceptible to landslides is the Carpathians. The reason for this is the nature of the relief and the geological structure. The high slopes combined with the flysch conditions render the Carpathians a region strongly prone to landslide occurrence. About 6% of the country is covered by the Carpathians, where 95% of all the landslides in Poland have been registered. In 2010, 50,000–60,000 landslides were recorded in the Carpathians, an average of one landslide per km^2 [7]. Landslide areas cover about 30–40% of the province areas in this region. The activation of numerous landslides in 2000 and 2010 by intense precipitation had disastrous consequences. Many residential buildings and road sections were destroyed [8]. There have been many cases of economic losses, which are estimated in millions of Polish zlotys. Some landslides are activated almost every year, which results in the destruction of residential and commercial buildings, transport infrastructure, transmission routes and agricultural and forest areas [9]. In agricultural areas, soil mixed with the layer located below presents inferior properties for agricultural production. The restoration of soil fertility in such areas is a long-term process [7]. Therefore, to mitigate the negative effects of landslides, it is necessary to effectively estimate landslide susceptibility and hazards [10,11].

From a mathematical perspective, landslide susceptibility mapping (LSM) presents the probability of landslide occurrence in a specific area based on an analysis of the terrain conditions and environmental conditions calculated from geo-environmental analysis. This describes the degree of proneness of specific terrain to landslides [12]. LSM is necessary for hazard assessment and the effective planning and management of regional sustainable development [13]. It is the subject of various studies worldwide [2,3,13–17]. The factors used for assessing landslide susceptibility are usually called Landslide Controlling Factors (LCFs). These factors are analyzed to create predictive models for landslide susceptibility, and they usually include topographical, geological, hydrological and environmental conditions. Effective LSM provides various land-use planners and decision makers with an opportunity to determine the regions appropriate for urban expansion and allows them to make the best possible use of land while avoiding landslide-prone areas [13,18].

Researchers all over the world have applied various methods for LSM. These methods can be qualitative or quantitative [14]. Qualitative methods are subjective and determine susceptibility heuristically, while quantitative methods involve the calculation of numerical measures, i.e., the likelihood of the occurrence of landslide phenomena in any susceptibility zone [12]. Among these quantitative approaches, the analytic hierarchy process (AHP) [14], the frequency ratio (FR) [14,19,20], the statistical index (SI) [20], the evidential belief function (EBF) [21], Dempster–Shafer (DS) analysis [22], logistic regression (LR) [19], the weights of evidence (WOE) model [20,21] and fuzzy logic (FL) [23] exist. Machine learning (ML) approaches have also been applied for LSM in the last few decades. Among them, the Support Vector Machine (SVM) [24,25], Artificial Neural Network (ANN) [19,21,23] and Random Forest (RF) [26] are increasingly used. The fundamental source for LSM with any of abovementioned methods is the landslide inventory map, which presents the location and extent of landslides.

Generally, when modeling terrain's susceptibility to land sliding, 70% of existing landslides are used for modeling and 30% are used for model validation [2,3,13,18,20–22,24,27], but some authors have even applied 80% of existing landslides for modeling purposes [19,28]. The landslides for modeling

are selected randomly across the entire study area, so they can capture a variety of conditions. This is a huge advantage in LSM. Unfortunately, there are still areas for which landslide inventory maps are simply not generated due to financial or reachability issues; they are not available in some hardly accessible areas. The authors of [29] presented a summary of the completeness of landslide inventories for various countries in Europe in 2012, which confirms that there are still areas for which landslide maps have not been generated. For example, landslide inventory in Poland has been generated step by step (commune area after commune area), and the generation of such an inventory sometimes proved to be very time consuming when the geological conditions were complex, resulting in a lack of landslide inventory in such regions. From another point of view in such a region, there is still the need for land-use planning, decision making, and the continuation of building and investment.

Considering this led to the following research question: could we assess landslide susceptibility in an area for which landslide inventory is not available but where it is available for the surrounding places? To answer this research question, we performed LSM based on so-called cross-modeling. More specifically, we divided our study area into two separate regions ("Łososina" and "Gródek") and performed modeling for the entire study area based on the "Łososina" and "Gródek" areas in the first and the second modeling scenarios, respectively. For the LSM, we utilized various topographical, geological and environmental LCFs together with the widely used Frequency Ratio method. LSM was performed in the study area greatly affected by landslide activity in the Polish Carpathians, in the area of the Rożnów Lake.

2. Materials and Methods

2.1. Study Area

The study area is located in the Outer Carpathians in the Małopolskie voivodeship. The main river of Dunajec is located in the study area, and Rożnów Lake was created as result of damming the Dunajec River. This dam is used in the Rożnów Power Plant [30]. The Rożnów water reservoir is one of the main elements for managing the water resources of the Dunajec river basin. (Figure 1). The study area covers from 49°40′ N to 49°46′ N latitude and from 20°38′ E to 20°48′ E longitude, which corresponds to 136 km^2 (Figure 1). Around 18.2 km^2 of this area is affected by landslides. According to Varnes' classification, updated by Hungr et al. [31], all landslides have a slide type of movement. According to Hungr's classification [31], within the Łososina commune, there are rock rotational slides (no. 6), clay/silt rotational/planar and compound slides (no. 11, 12, 14). Unfortunately, the landslide inventory provided by Polish National Geological Institute does not represent more detailed characteristic of landslide types e.g., shallow/deep-seated landslides or planar/rotational slides. Generally, landslides are classified as deep or shallow based on the material, movement mechanism and depth of the rapture surface [32]. The authors of [33,34] reported that landslide is considered as shallow when the depth of the sliding plane is less than 10 m and deep seated when sliding plane is deeper than 10 m. When investigating sizes [35,36], characteristics and slip depth of some landslides described in the landslide inventory documentation [37,38], we can concluded that shallow as well as deep seated landslide exists in investigated region. Generally in this region, landslides are slow- to very-slow-moving. The study area mainly consists of Eocene–Oligocene sandstones and shales and Upper Cretaceous sandstone and conglomerate–Lower Stebna layers. This is one of the most landslide-affected areas in Poland. Additionally, due to the complex geological conditions, landslide inventories in this region of the eastern shore of Rożnów Lake were unavailable for a long time. Thus, its situation suited the research question of this paper.

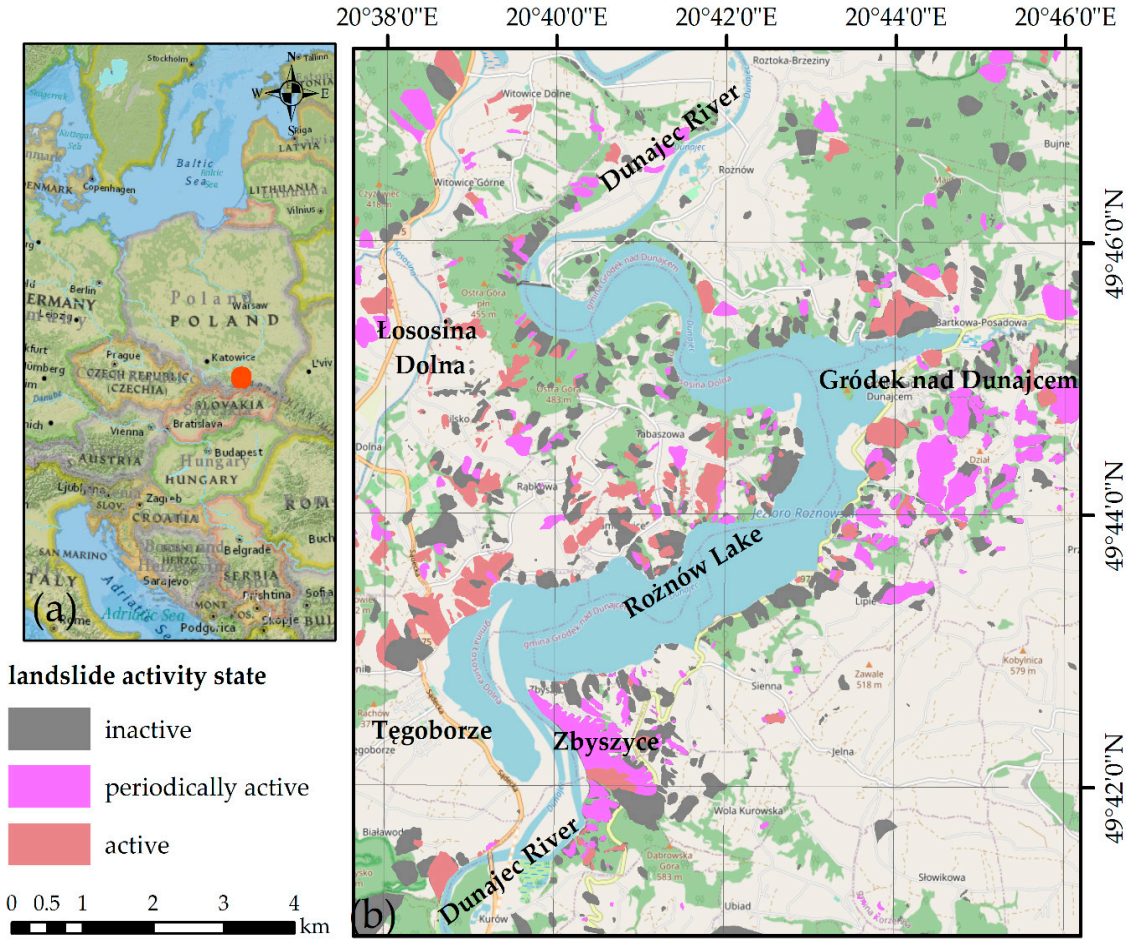

Figure 1. Location of the study area and (**a**) existing landslides and (**b**) their activity state.

2.2. Methodology

The methodology flowchart is presented in Figure 2. The study area was divided into two regions called "Łososina" and "Gródek", separated by Dunajec River (also the boundary of the Łososina and Gródek communes). These regions were used for cross-modeling. This means that in the first model, "Łososina" was used for modeling, while in the second, "Gródek" was used for the modeling of the landslide susceptibility of the entire study area. The official national landslide inventory map (SOPO) was used for LSM. The Frequency Ratio (FR) method was applied as a tool for landslide modeling. The susceptibility assessment was performed in the same manner by using various landslide input data. Based on this, a direct comparison between these two strategies was possible. More detailed descriptions of data and methods used are presented in the following subsections.

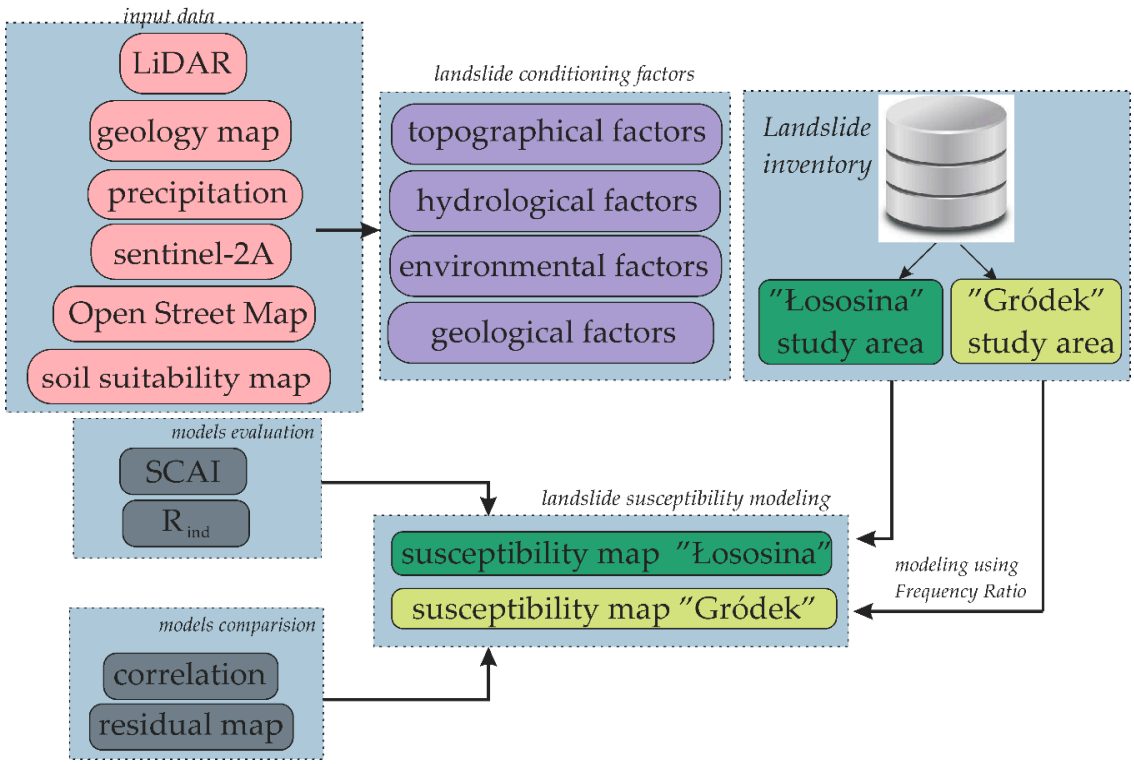

Figure 2. Conceptualization of the applied methodology (SCAI: Seed Cell Area Index).

2.3. Input Data

The landslide inventory database (SOPO) from the Polish National Geological Institute was used for the input data (Figure 1). These data allowed the generation of models and validation datasets. The existing landslide locations and boundaries within the SOPO database were captured using conventional techniques, mostly comprising field reconnaissance, the visual interpretation of aerial photographs, and the analysis of historical data [39]. The landslides within the study area are stored in the SOPO database and were mapped during field work in the years 2010, 2011, 2012, 2013, 2014 and 2015 [35,37,38,40]. Additional mapping was also performed on the basis of topographic maps at a 1:10 000 scale, supported by stereoscopic analyses of aerial photographs and LiDAR data [9].

Various Landslide Conditioning Factors (LCFs) were generated from the data captured from different sources. Table 1 presents the data sources used to create so-called second-order input data such as the Digital Elevation Model (DEM), geological and soil map etc. The LiDAR data were acquired within the framework of the IT System of the Country Protection (ISOK) project. Almost the entire area of Poland has been scanned for the implementation phase of the extraordinary hazard (mostly water hazard) protection system (ISOK project) [41]. A point cloud with a density of 4–6 points/m^2 was generated, and the calculated Root Mean Square Error was about 0.15 m for the height coordinate [41]. This LiDAR point cloud was subsequently used for DEM generation. To decrease the data volume and discard some of the artefacts from the original DEM, we followed the recommendations of [42–44] and generated a DEM with a resolution of 2 m. This approach appears to be common among various papers, and many authors have reported that the finest DEM resolution is not always the best choice [42–45]. Based on the DEM, topographical LCFs were subsequently generated as described in Section 2.4.

A Sentinel-2A image acquired via the Copernicus Scientific data hub was used to extract the boundary of Rożnów Lake. This shape was extracted by the calculation of the Normalized Difference Vegetation Index (NDVI). More specifically, an NDVI value lower than 0 was used to extract the shape of the lake, based on which another LCF was calculated (the lake proximity). Moreover, an agricultural soil map acquired from the geoportal of the Małopolskie voivodeship was used to generate a soil-suitability map. A geological map was also obtained from the Polish National Geological Institute.

As well as the geological map, the soil maps were digitized and stored as vector layers in ArcGIS (version 10.6, ESRI, Redlands, CA, USA). Additionally, a thrust and fault network was generated based on previous work [30] via a digitization process. The road network was acquired from OpenStreetMap (OSM). Because the river network in OSM is very sparse, the stream network was extracted with the DEM, with which the flow accumulation and direction were initially calculated. The subsequent thresholding of the flow accumulation values allowed the extraction of the stream network. Finally, this network was manually refined and converted into the vector layers. Because precipitation is a direct trigger of landslides worldwide, we downloaded the precipitation measurements from four different meteorological stations in this area. We utilized measurements from 2019 due to the changes of the weather conditions caused by the climate change. From one year to another, we observed much more extreme weather phenomenon. Thus, to represent the most real and current rainfall situation, we applied the rainfall measurement from 2019. A precipitation map was generated based on these measurements by inverse distance weighted interpolation. A summary of all the data used in this study is presented in Table 1.

Table 1. Second-order input data generation from various data sources (DEM: Digital Elevation Model, ISOK: IT System of the Country Protection, NDVI: Normalized Difference Vegetation Index).

Generated Second-Order Input Data	Method	Data Type	Data Source	Link
DEM	Ground point extraction (class = 2)	LiDAR	ISOK	https://isok.gov.pl/hydroportal.html
Stream network	Flow direction and flow accumulation analysis	Shapefile	DEM	————
Geology map	Digitalization	Raster	Polish National Geological Institute,	https://geolog.pgi.gov.pl/
Rożnów lake shapefile	NDVI < 0	Sentinel-2A satellite image (25 March 2020)	European Space Agency	https://scihub.copernicus.eu/
Land cover map	Maximum Likelihood Classification	Sentinel-2A satellite image (25 March 2020)	European Space Agency	https://scihub.copernicus.eu/
Road network	-	Shapefile	OpenStreetMap	https://download.geofabrik.de/
Soil Suitability Map	Digitalization	Raster	Małopolska Spatial Information infrastructure	https://miip.geomalopolska.pl/
Fault and thrust network	Digitalization	Raster	[30]	[30]
Precipitation	Inverse distance weighed interpolation	Precipitation measurement in meteorological stations (points)	Institute of Meteorology and Water Management	https://danepubliczne.imgw.pl/

2.4. Preparation of Landslide Conditioning Factors

From the DEM generated from LiDAR data, various topographical layers were generated (LCFs). Table 2 presents an overview of various widely applied LCFs generated from the DEM and Figure 3 presents a graphical representation of some of the used LCFs. Based on some DEM analysis, hydrology-related layers were also extracted: the compound topographic index (CTI), integrated moisture index (IMI) and flow direction (FD). To create accurate LSM, we also generated a stream proximity layer based on the stream network extracted from the DEM (see Section 2.3) and Euclidian Distance Buffering (EDB) tool within ArcGIS.

The additional auxiliary data presented in the previous subsection and Table 1 made the generation of additional geological, hydrological and environmental factors possible. Among them, tectonics, lithostratigraphy and faults and thrust proximity were possible to generate by utilizing the geology map and [30]. The Normalized Difference Vegetation Index (NDVI) and lake proximity layers were created from the Senitel-2A data acquired on 25 March 2020. The lake proximity was generated based on Euclidian distance buffering and the lake shapefile extracted from the NDVI (Section 2.3). The Sentinel-2A data were also used to create a Land Cover (LC) map by supervised classification using the Maximum Likelihood (ML) approach and the Sentinel-2A spectral bands. The Overall Accuracy

(OA) of this LC map was assessed by comparing ground truth samples with the classification results, indicating that the OA of our map was approximately 94%—sufficient for this study. The shapefile of the road network was captured from OpenStreetMap, and similarly to previous distance-related layers, the distance to road layer was created. The soil suitability layer, which presented complexes of agricultural soil suitability, was created based on the digitalization of the soil suitability map.

Table 2. Landslide conditioning factors used in presented study (ML: Machine learning).

Variable	Data Used	Technique	Classification Method	References
elevation	DEM	—	Natural Jenks	[2,3,13–15,19,22,26,46]
aspect	DEM	ArcGIS	Natural Jenks	[13,14,21,22,24,26]
slope	DEM	ArcGIS	Natural Jenks	[2,3,13–16,19–22,24]
curvature	DEM	ArcGIS	Natural Jenks	[3,13,15,16,18,20,21,24]
side exposure index (SEI)	DEM	[47]	Natural Jenks	[45]
tectonics	geology map	—	—	[3,13,14,19,20,22,48]
lithostratigraphic unit	geology map	—	—	[19,27]
fault proximity	geology map	EDB	Natural Jenks	[13,19–22,24,26]
thrust proximity	geology map	EDB	Natural Jenks	[49,50]
distance to streams	DEM	EDB	Natural Jenks	[3,13,19,20]
distance to lake	Rożnów lake shapefile	EDB	Natural Jenks	[16,24]
compound topographic index (CTI)	DEM	[47]	Natural Jenks	[13,48,51,52]
integrated moisture index (IMI)	DEM	[47]	Natural Jenks	[46,53]
flow direction	DEM	[47]	Natural Jenks	[45,54]
precipitation	measurements from meteorological stations		Natural Jenks	[13,51,55]
distance to roads	road network	EDB	Natural Jenks	[3,13,14,16,19,22,24,28,51]
Land Cover (LC)	Sentinel-2A	Supervised ML classification	—	[2,3,13,28,51]
NDVI	Sentinel-2A	$\frac{NIR-RED}{NIR+RED}$ where NIR is near inferred band (band 4) and RED is the red band (band 3)	Natural Jenks	[3,13,24,28,51]
soil suitability	digitized soil map		—	[3,13,21,24,28,51]

2.5. Landslide Susceptibility Modeling

To fully achieve the goal of this study, we used various data for landslide susceptibility assessment. Namely, we generated the two landslide susceptibility models based on landslides located within the "Łososina" and "Gródek" regions in the first and second modeling scenarios, respectively. The qualitative information about the number of landslides used for modeling and its contribution in the total analyzed area is presented in Table 3. A graphical representation of the region separation is presented in Figure 4. Based on this, it can be observed that 46% and 54% of the total detected landslides were used for the LSM in "Łososina" and "Gródek" strategies, respectively. Moreover, it is apparent that there is an 8% difference in the landslides used for modeling between these two strategies. At this point, it is worth reiterating that 70% of the landslides are typically used for LSM in the literature [2,3,13,18,20–22,24,27]. Moreover, a random sampling strategy is used for assessing landslide susceptibility; the landslides used for modeling are distributed randomly and evenly across the investigated area, so the variety of conditions (LCFs) can be better captured. Considering this, in the first and second strategies, we used fewer landslides for modeling purposes. Thus, we supposed that this modeling of landslide susceptibility would have lower performance than that usually presented in the literature. However, the goal of the presented work was to investigate whether landslide inventory could be used for LSM in surrounding regions rather than to strive for accuracy.

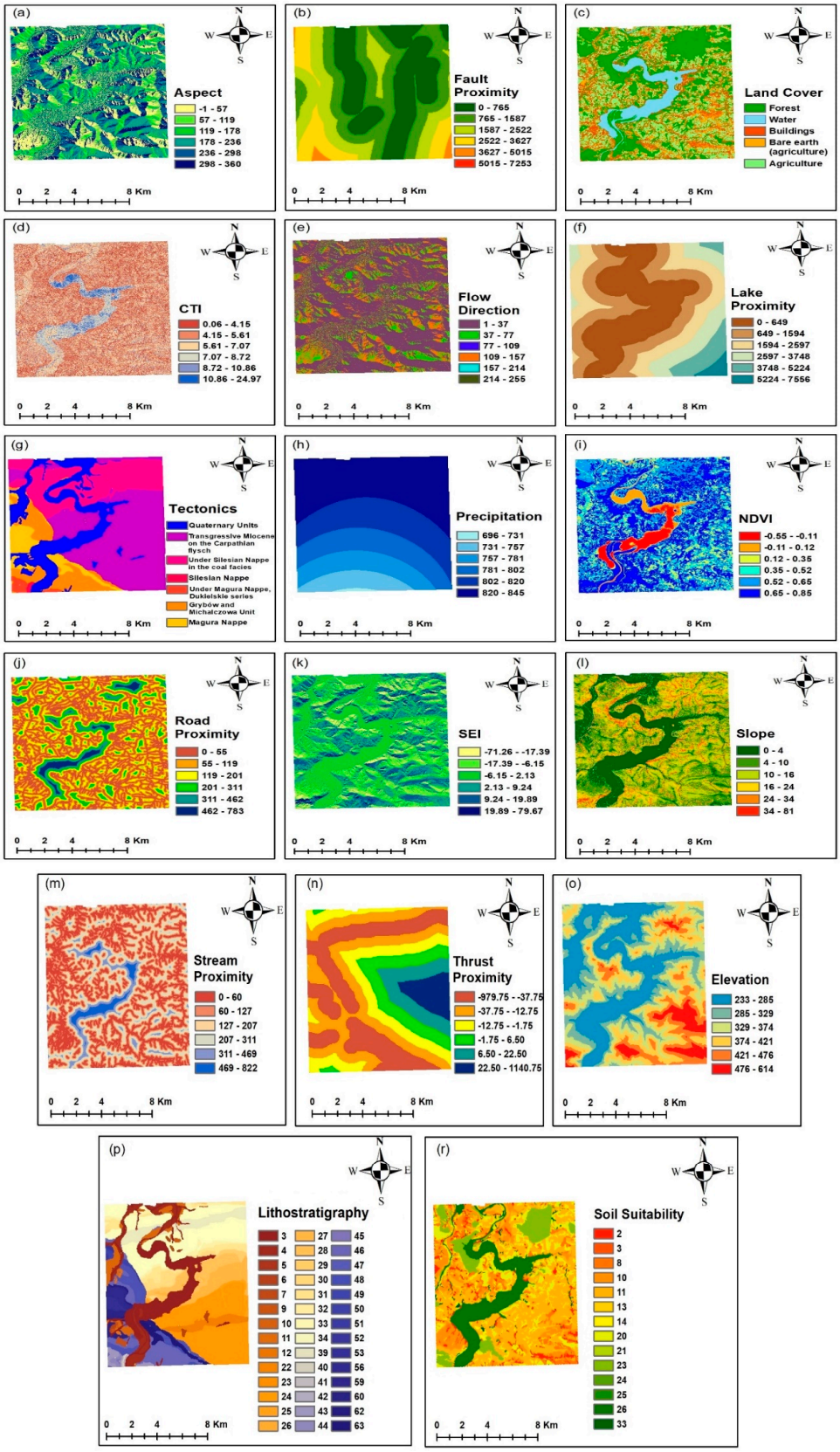

Figure 3. Examples of landslide conditioning factors utilized in this study (**a**) aspect, (**b**) fault proximity, (**c**) land cover, (**d**) CTI, (**e**) flow direction, (**f**) lake proximity, (**g**) tectonics, (**h**) precipitation, (**i**) NDVI, (**j**) road proximity, (**k**) SEI, (**l**) slope, (**m**) stream proximity, (**n**) thrust proximity, (**o**) elevation, (**p**) lithostratigraphic units, (**r**) soil suitability.

Table 3. Landslides used for landslide susceptibility modeling in various strategies.

Strategy	Map	Study Area	No of Landslide in Total Study Area	Landslide Area in Total Study [km^2]	Percentage of Total [%]
1st strategy	SOPO	Łososina	322	8.31	46
2nd strategy	SOPO	Gródek	425	9.94	54
		Total study area	747	18.25	—-

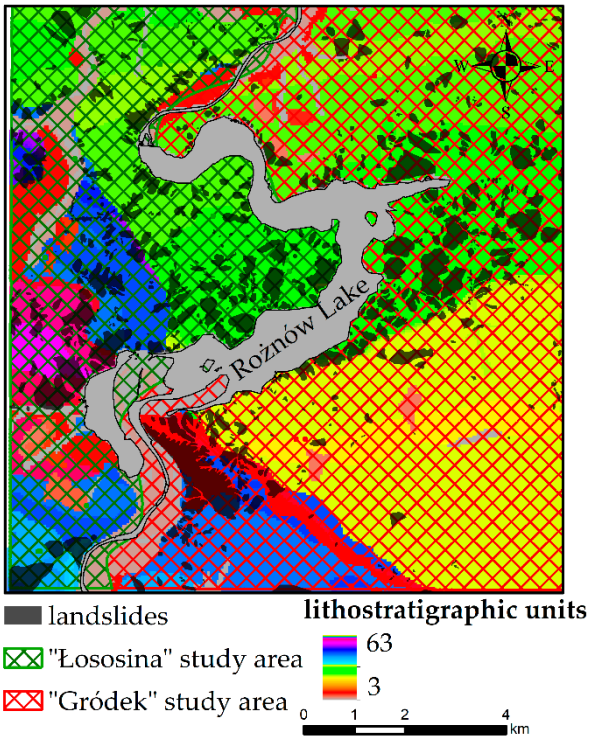

Figure 4. Study area division into "Łososina" region and "Gródek" region superimposed on lithostratigraphic units.

2.6. Application of Frequency Ratio Model for Landslide Susceptibility Zonation

The Frequency Ratio (FR) is a geospatial assessment tool used to estimate the susceptibility to landslides in a given research area [13]. It belongs to the bivariate statistical methods, and its value depends on the relationship between the location of landslides and LCFs [27]. For LCFs, weights are assigned based the ratio of the number of observed landslides to the area of the study area. The weights, represented as FRs, can be calculated using landslide inventory and each specific LCF [27]. When j is the class of a specific LCF (i), the FR is defined by the following equation:

$$\mathrm{SCAI}_i = \left(\frac{E_i}{F_i}\right) \quad (1)$$

where:

A = the number of pixels of the landslide in each LCF class
B = the total number of pixels of the landslide in the test area
C = the number of pixels in each LCF sub-class
D = the total number of pixels in the test area [1]

Accordingly, the FR was calculated by overlying landslide pixels with the thematic layers or LCF layers presented in Section 2.4 Values obtained using this method greater than 1 imply high landslide susceptibility within this class [13] and a strong correlation between the landslide occurrence and LCF class [28]. Values below 1 indicate no or a slight correlation between the LCF and landslide occurrence [13,28].

The Landslide Susceptibility Index (LSI) was subsequently calculated for each pixel in the image (x,y) according to the formula:

$$\mathrm{LSI}_{xy} = \sum_{i=1}^{n} \mathrm{FR}_{i,j} \tag{2}$$

Based on natural breaks, Jenks [56] developed an optimization method to minimize within-class variance while maximizing between-class variance. This classification method is generally implemented into GIS software, such as ESRI@ ArcGIS software or QGIS (free open source software). The classes are split according to natural clusters inherent in the data, and the boundaries are statistically determined when relatively large jumps occur within the susceptibility indices as determined by their variance. The LSI values were separated based on this method into five susceptible classes. This number of susceptibility zones is commonly used in small-scale landslide susceptibility mapping [57,58]: very low, low, moderate, high and very high. These are considered adequate for revealing any spatial patterns preserved in a dataset and aiding the interpretation of these LSMs [59].

2.7. Methods for Model Validation

Model validation is a crucial step that indicates whether the generated model achieves a certain level of accuracy. Without accuracy assessment, generated models are meaningless [13]. We applied the Seed Cell Area Index (SCAI) and Relative Landslide Density Index (R_{ind}) to evaluate our landslide susceptibility maps in this study. We also calculated a residual map and correlation index between two susceptible maps. The SCAI and R_{ind} were calculated for validation and modeling areas for both models.

2.7.1. Index of Relative Landslide Density

Bearing in mind that the LSM value was used to distinguish susceptible and non-susceptible areas, landslides may be expected to occur in areas with more susceptible zones [60]. A relative landslide density index (R_{ind}) was calculated to verify this. This index is defined by the ratio of the landslide area and given susceptibility class to the overall landslide density. The index takes the following form:

$$R_{ind} = 100 \cdot \frac{n_i / N_i}{\sum n_i / N_i} \tag{3}$$

where:

n_i = the number of landslides observed in a susceptibility class

N_i = the area covered by the cells of this class [61].

2.7.2. Seed Cell Area Index

The Seed Cell Area Index (SCAI) validation technique used in this study was developed by Süzen and Doyuran [62]. It is described as the ratio between the percentage of pixels of the exact class of landslide susceptibility and the percentage of the pixels of existing landslides in a given landslide susceptibility zone. The SCAI is assumed to be a reliable validation technique [13,14]. If its values decrease from very low to very high classes of LS, the model is regarded as excellent [13]. When i is the specific susceptibility map, SCAI is represented as follows:

$$\mathrm{SCAI}_i = \left(\frac{E_i}{F_i} \right) \tag{4}$$

where: E_i= percentage of landslide pixels in specific susceptibility class to total landslide pixels F_i= percentage of pixels in specific susceptibility class to total image pixels.

2.7.3. Map/Model Comparison

To evaluate the reliability of the two susceptibility maps generated based on two different landslide input datasets, we performed model or map comparison. Firstly, we determined the raster difference between these two maps, showing how these two maps differed from each other. By comparing two models with different susceptibility zones, a so-called residual map was generated [63]. This residual image showed how pixels shifted from one landslide susceptibility class to another between these two maps. Thus, a residual image can have a maximum five different classes: no difference, one-zone difference (1, −1), two-zone difference (2, −2), three-zone difference (3, −3) and four-zone difference (4, −4) [14]. We also calculated the Pearson correlation coefficient between these two landslide susceptibility maps to evaluate their similarity.

3. Results

This section comprises the following three subsections: (1) the spatial relationship between landslide and conditioning factors, and the FR indexes used for the LSI calculations (presented in Appendices A and B); (2) a presentation of the landslide susceptible maps generated by two models; and (3) the validation and comparison of the generated models using the SCAI, R_{ind} and model comparison.

3.1. The Spatial Relationship Between Landslide Locations and Analyzed Landslide-Controlling Factors

The frequency ratios for the first and second models are presented in Appendices A and B, respectively. Observing the FRs, it is apparent that the topographic factors were not of great importance for the preparation of the LSM in this study. To the contrary, it can be observed that the lithostratigraphic units were more important than tectonics or other geological or environmental conditioning factors. For clarity, the ten highest frequency ratios achieved for each model are shown in Figure 5, from which it is clear that the lithostratigraphic units were the most important variable in both models. Soil suitability also played an important role in landslide occurrence. In the "Łososina" model, precipitation and tectonic were also important landslide-controlling factors.

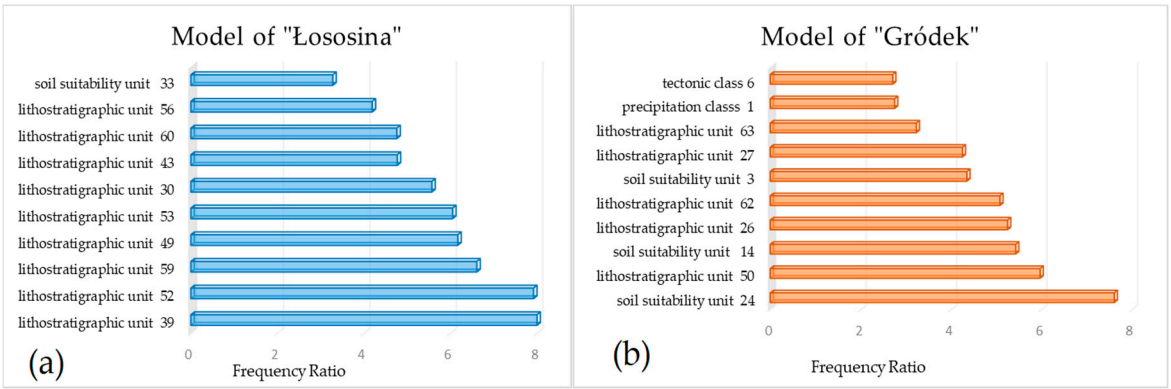

Figure 5. Importance of landslide conditioning factors in landslide susceptibility mapping (LSM) based on (**a**) "Łososina" and (**b**) "Gródek".

3.2. Landslide Susceptibility Maps

The LSIs were calculated as described in Section 2.5 based on the FRs presented in Appendices A and B and afterwards sorted into five susceptibility classes by Natural Jenks classification. Figure 6a,b present various LSIs calculated for the model based on "Łososina" and based on "Gródek", respectively. Similarly, Figure 6c,d present the susceptibility classes (SC) for the model based on "Łososina" and that based on "Gródek", respectively.

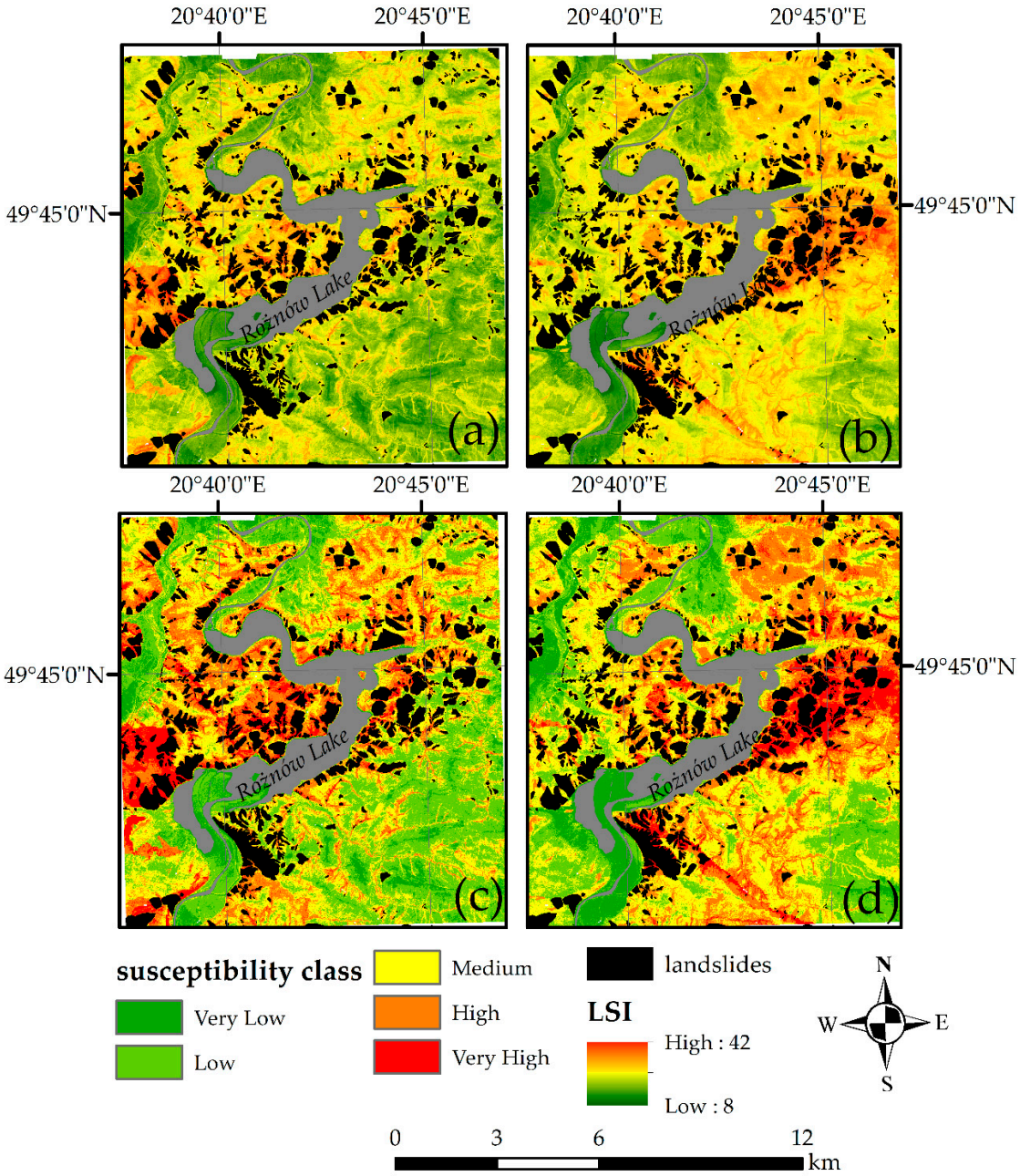

Figure 6. Landslide Susceptible Index (LSI) and landslide susceptibility zones for the (**a**,**c**) "Łososina"-based model and (**b**,**d**) "Gródek"-based model.

The results from the "Łososina" model show that the very low, low, moderate, high and very high landslide susceptibility zones of the LSM cover 5%, 10%, 28%, 31% and 26% of the investigated study area, respectively (Figure 7a). The "Gródek" model results show that the very low, low, moderate, high and very high landslide susceptibility zones of the LSM cover 7%, 20%, 35%, 28% and 10% of the investigated study area, respectively (Figure 7b). From these indices, the same quantity can be observed for very high and high susceptible classes. Some relatively high differences can be observed within the low susceptibility class.

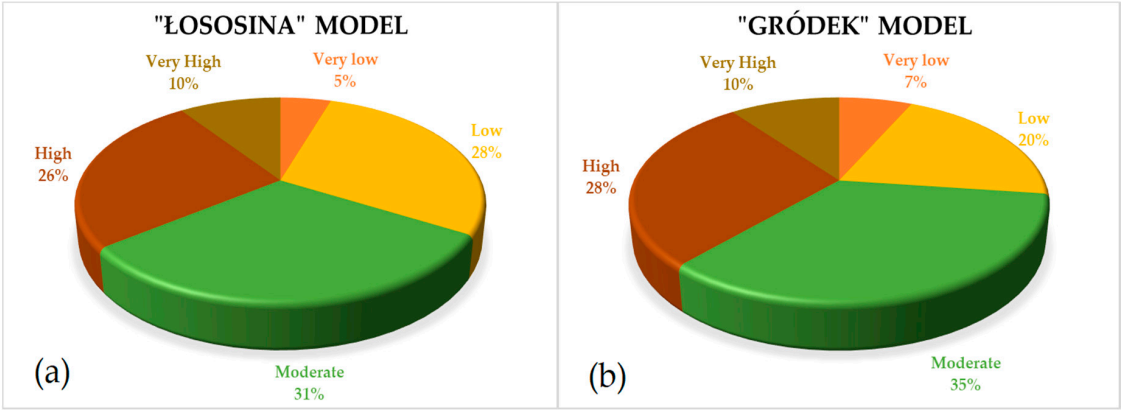

Figure 7. Distribution of susceptible classes across the study area for the (**a**) "Łososina"-based model and (**b**) "Gródek"-based model.

3.3. Evaluation of Landslide Susceptibility Models

3.3.1. Seed Cell Area Index

We evaluated the achieved susceptibility models based on the SCAI index; however, our evaluation was performed for split areas ("Łososina" and "Gródek"). This allowed for the better investigation of possible changes (the modeling and validation splitting strategy are described in Section 2.5). If the values of the SCAI decrease from very low to very high classes of LS, the model is regarded as excellent [13]. Table 4 presents percentage of each susceptible class, landslide observed in this specific class and SCAI index for both models. We can observe that based on the evaluation of the LSM in the modeling area, the SCAI index was extremely high (2491) and extremely low (0.42) for the "very low" and "very high" susceptible zones, respectively. These are exceptionally good results. A somewhat lower performance can be observed for the LSM based on "Gródek" and evaluated in the "Gródek" area; however, even its results were largely correct. Moreover, based on the evaluation of our results in the validation area, the SCAI index for the "very low" class in both cases ("Łososina" and "Gródek" model) was higher than 50, and it was below 0.5 for the "very high" susceptibility class, which is also considered appropriate.

Table 4. Landslide susceptibility model evaluation based on modeling and validation study areas.

Model/ Modeling Area	Class	Validation Area	Pixels in Domain	%	Landslide Pixels within the Specific Class [km^2]	Percentage of Total [%]	SCAI
Łososina	Very low	Łososina	630,917	0.06	46	0	2491.70
	Low		2,064,901	0.18	11,417	0.01	32.86
	Moderate		2,900,312	0.25	213,545	0.10	2.47
	High		3,515,091	0.31	841,964	0.41	0.76
	Very High		2,323,889	0.20	1,010,439	0.49	0.42
	Very low	Gródek	877,306	0.04	1645	0	66.82
	Low		6,874,753	0.35	144,129	0.06	5.98
	Moderate		6,843,835	0.34	907,641	0.37	0.94
	High		4,534,307	0.23	1,173,528	0.47	0.48
	Very High		713,775	0.04	259,295	0.10	0.34

Table 4. *Cont.*

Model/ Modeling Area	Class	Validation Area	Pixels in Domain	%	Landslide Pixels within the Specific Class [km^2]	Percentage of Total [%]	SCAI
Gródek	Very low	Gródek	894,142	0.08	1006	0	194.50
	Low		3,390,427	0.30	22,136	0.01	33.48
	Moderate		6,373,115	0.56	324,619	0.13	4.27
	High		6,344,671	0.55	953,086	0.38	1.45
	Very High		2,841,621	0.25	1,185,391	0.48	0.52
	Very low	Łososina	1,236,346	0.11	3176	0	70.74
	Low		2,948,451	0.26	196,954	0.09	2.72
	Moderate		4,448,486	0.39	924,964	0.45	0.87
	High		2,431,304	0.21	786,222	0.38	0.56
	Very High		370,523	0.03	166,095	0.08	0.41

3.3.2. Index of Relative Landslide Density

The values of relative landslide density index R_{ind} calculated for high and very high susceptibility classes are presented in Table 5. It can be observed that the R_{ind} calculated for the area used for modeling is very high for both models (90% and 86%). For the validation areas, located on the other side of the river, the R_{ind} are significantly lower (57% and 46%). This indicates changes in accuracy according to landslide susceptibility. Therefore, for the better investigation of the model performance, R_{ind} should also be taken into account beside the SCAI index.

Table 5. R_{ind} calculated for very high and high susceptibility classes.

	R_{ind}	
Area	**"Łososina" [%]**	**"Gródek" [%]**
"Łososina" area	90	46
"Gródek" area	57	86
Total	72	68
Total average	70	

3.3.3. Map/Model Comparison

To better investigate the similarity of the models, we calculated the LSI and susceptible zone difference between them (Figure 8). The residual maps present the differences in the LSI and susceptibility zones. Five differences in the susceptibility classes can be distinguished (0–4 zones difference), as presented in Table 6. Green color represents no difference in the susceptible zones between these two models, while light red and light blue represent one susceptible zone difference (1,−1). According to Table 6 almost half of the map (47%) presents no difference in landslide susceptibility zones, and 42% differs in one susceptibility zone. Based on the difference between the left and right images, it can be seen that negative and positive values exist between these two sides of the study area, respectively (Figure 8). This is because the "Łososina" model was adjusted to the "Łososina" area and the "Gródek" model was adjusted to the "Gródek" area.

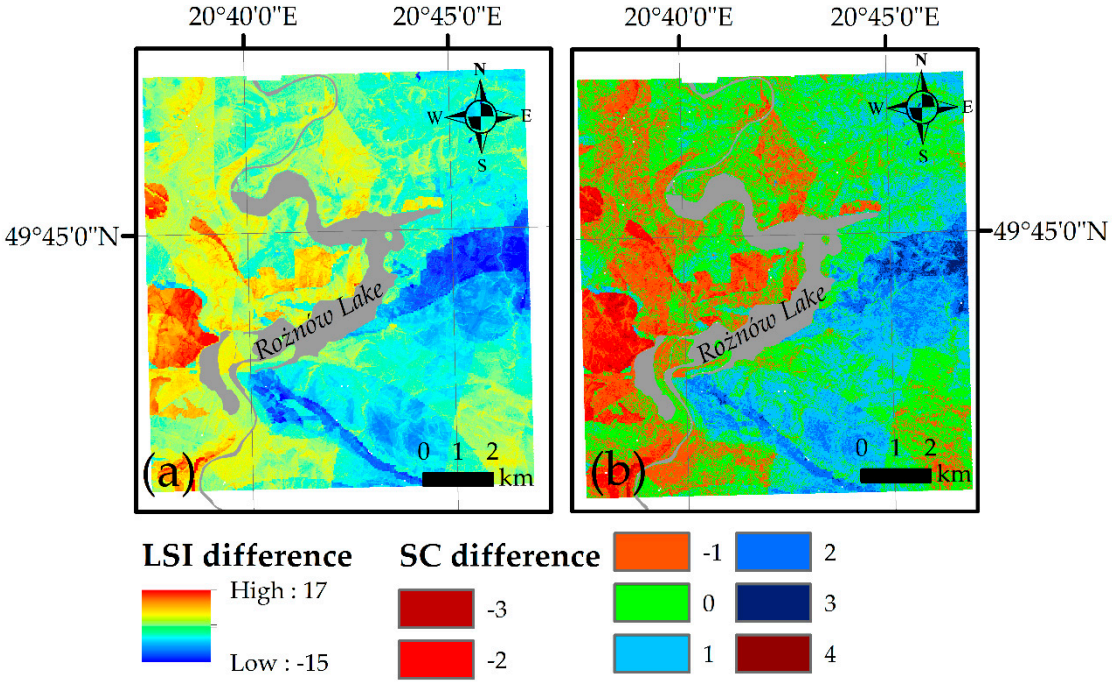

Figure 8. Difference between "Łososina" model and "Gródek" model for (**a**) Landslide Susceptibility Index (LSI) and (**b**) susceptible class (SC).

Table 6. Difference between two susceptibility models.

	Difference between Models of "Łososina"and "Gródek"	
	Pixels	**Area Percentage [%]**
no difference	13,031,043	47
one-zone difference	14,623,961	42
two-zones difference	3,219,848	10
three-zones difference	405,072	1
four-zones difference	751	0
Correlation (*r*)	0.697	

The correlation index calculated for both susceptible maps is 0.697. This value is quite similar to the total average landslide density in the high and very high susceptibility zones for the entire study area (compare with Table 5). Therefore, the overall accuracy of both of these susceptibility maps for the entire investigated region can be estimated at 70%. However, it must be mentioned that the accuracy changes from region to region. In the area where the landslides used for modeling are located, 90% accuracy can be expected, while in the area where the landslides used for modeling are not preserved (validation area), an LSM accuracy between 46% and 57% can be expected.

4. Discussion

Based on a comparison of the SCAI indices, the general performance (in terms of accuracy) of both models can be described as good. For the validation study area, the SCAI index was higher than 50 and lower than 0.5 for the very low and very high susceptibility classes, respectively. This shows higher performance than that described in other studies [13,14,55]. The R_{ind} calculated for the validation area shows that 46% and 57% of landslides fall into the high and very high susceptibility zones in the "Gródek" and "Łososina" models, respectively. This implies that besides the SCAI index, the R_{ind} should also be used to evaluate the LSM. The explanation for the low value of R_{ind} for the high and very high classes is that 37% and 45% of the landslides are located in the moderate class in the "Łososina" and "Gródek" models. This indicates that another classification method should be

considered to effectively differentiate the susceptibility zones (e.g., quantiles, IsoData). This issue has been discussed in [60].

When comparing these two models, the SCAI indexes for Łososina model are more satisfactory. This is mostly due to the high SCAI values for very low and low susceptible zones and very low values for high and very high susceptible zones. Moreover, relative landslide density (R_{ind}) is higher for Łososina model (72%). Therefore, this model is more reliable than the Gródek model ($R_{ind} = 68\%$). This is surprising because it was expected that the "Gródek" model would better predict landslide susceptibility due to the greater amount of landslide used for modeling (54%) when compared with "Łososina" model (46%). Nevertheless, this indicate that the greater amount of landslides used for modeling does not go hand in hand with improved landslide susceptibility assessment.

As we mentioned in the Introduction section, scientists applied a randomly selected 70% of the landslides for modeling and 30% for validation. In the selection strategy, the landslides used for the modeling are distributed across the study area. Instead of our sampling strategy (splitting the area for the modeling and validation regions), landslides distributed evenly across the image can better "capture" a variety of topographical, geological and other environmental conditions (LCFs). When the study area is split into modeling and validation areas, it is possible for some landslide-prone geological units to be absent from the area used for modeling. Additionally, by comparing Figure 8 with LCFs, it can be observed that differences of up to two or three susceptible zones occur in the areas of faults and thrust proximity (intensive red and blue color). These differences of two classes can also be observed in changes of lithostratigraphic units (intensive red and blue color). This additionally confirmed our notion that the landslide sampling strategy had a crucial effect on the accuracy of LSM.

To better investigate the difference between these two models, a correlation matrix between the difference in the LSI index (Figure 8a) and each LCF was calculated and is presented in Figure 9. Based on this, it can be concluded that this difference between the models highly corresponds to the fault, lake, and trust proximity. It can therefore be deduced that the landslides used for modeling did not capture the variability of geological (thrust and fault proximity) and environmental (lake proximity) conditions. Landslides that are better distributed across the entire study area can better describe the variety of geological and environmental conditions (e.g., thrust, fault and lake proximity) and therefore better predict landslide susceptibility.

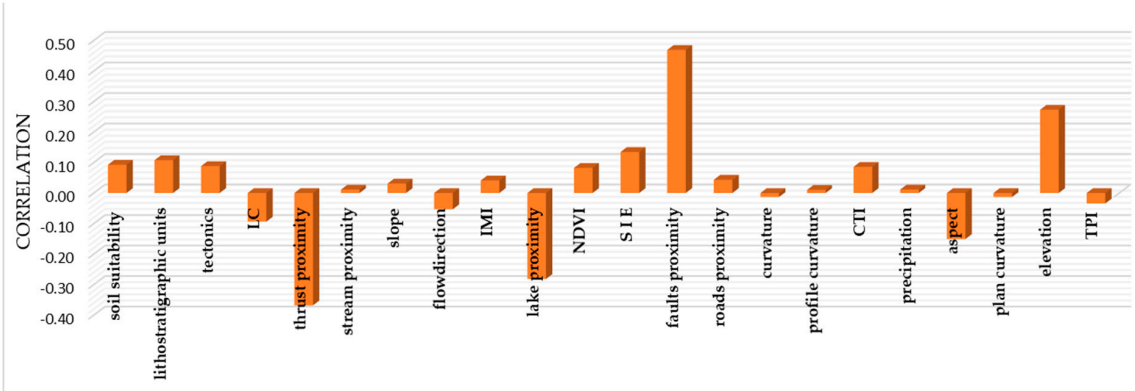

Figure 9. Correlation index between raster representing LSI difference between two susceptible models and each landslide-conditioning factor (LCF) (LC: Land Cover, IMI: Integrated Moisture Index, SEI: Side Exposure Index, CTI: Compound Topographic Index, TPI: Topographic Position Index).

This outcome answers our research question whether we can perform LSM in an area for which a landslide inventory is not available but where such an inventory is available for the surrounding region. Based on this study, we can infer that the assessment of landslide susceptibility based on surrounding landslide inventories cannot be effectively performed in the areas when the geological and environmental conditions have changed. Generally, based on the results in Table 6, there is a 47%

chance of being correct with the susceptibility zone and a 42% chance of error with one susceptibility zone. Therefore, we can generally perform landslide susceptibility modeling based on the landslide inventory for a neighboring region. However, it should be reiterated that there is 10% chance of our susceptibility map differing from target landslide susceptibility of two zones in some areas. These are generally located in areas with significant changes in the geological or environmental conditions. In this case, when we considered only very low susceptible classes for the decision making, this susceptibility map can be used for decision making and planning.

Another aspect which should be discussed here is the variability of landslide type used for LSM. Since the information about the specific landslide type (shallow/deep seated or planar/rotational) is not available within the national inventory, all landslides were used for LSM. A lack of differentiation between landslide types used for LSM is practiced by many researchers [3,13,14,22,55,61,62]. However shallow and deep seated landslides differ in terms of damage influence, size and volume [64]. Deep seated landslides generally appeared due to the relationship between natural denudation process and long-term rainfall, whereas, shallow landslides are related to short high-intensity rainfall [64]. Therefore, at this moment it is unknown whether high correlation between LSM difference (Figure 8a) and geological factors (faults and thrust proximity) correspond to some specific characteristic and mechanism of deep seated landslides, which are known for their strong connection with geology. Thus, in future works it is worth considering differentiation of landslide type (shallow/deep seated) in susceptibility modeling and its relation with landslide conditioning factors.

5. Conclusions

The fundamental source for LSM is landslide inventory. Unfortunately, there are still areas for which landslide inventories are not generated due to financial or reachability constraints. Thus, this study evaluated whether landslide susceptibility could be effectively assessed in such areas where landslide inventory was available for an adjacent region. Having considered the results from the two landslide susceptibility maps generated by cross-modeling, we can assert that susceptibility zones generated based on inventory located in an adjacent region will be different for 53% of the analyzed area when compared with a susceptibility map generated using landslide inventory. On the contrary, it can be estimated that 47% of the map generated based on inventory for a surrounding area will be similar to a map generated in a traditional manner (using landslide inventory for the analyzed region).

Based on a comparison of the accuracy measures for the training and validation areas, we can conclude that the cross-modeling of landslide susceptibility has great influence on the accuracy of landslide susceptibility determination. This is directly connected with sampling strategy (landslide selection for susceptibility modeling). In this study, we applied a sampling strategy completely different to that widely presented in the literature [13,14,20,55]. Namely, we performed cross-modeling based on landslides located in the cluster (Łososina/Gródek region) defined by the specific natural boundary (Rożnów Lake and Dunajec River). In the LSM literature, the landslide events used for modeling are usually randomly and evenly distributed across the study area. This allows capturing of the variety of geological conditions and the susceptibility to landslides. Therefore, in a perfect scenario, it is desirable to use landslides distributed evenly across the study area and located in various geological settings. This will introduce the effect of autocorrelation and allow the effective assessment of landslide susceptibility.

Nevertheless, when such a landslide sampling strategy is not possible due to the lack of landslide inventory, landslide susceptibility can be assess based on landslide inventory available in adjacent region. However, discrepancies between these two models exist in the areas of critical geological structures (thrust and fault proximity), and the reliability for such susceptibility zones can be low (2–3 susceptibility zone difference). Nonetheless, such areas cover only 11% of the analyzed area; thus, we can conclude that in remaining regions (89%), LSM generated by the inventory for the surrounding area can be used. Still, the low reliability of such a map in areas of critical geological structures should be borne in mind. This applies to LSM in other regions where the geology can be much more complex.

As such, the discrepancies among the LSMs generated based on the strategy presented in this study are particularly relevant given that the overestimation or underestimation of susceptibility can have crucial effects on land-use management and civil protection planning. The optimal map should be able to depict most potential landslide events and, at the same time, be effective and accurate for preventing failures in the study area. Therefore, specific landslide inventory is certainly needed to more reliably estimate landslide susceptibility in complex geological areas.

Author Contributions: Conceptualization, K.P.-F.; experiments, K.P.-F., N.O., M.P.; data capture, K.P.-F.; formal analysis, K.P.-F., N.O., M.P.; validation, K.P.-F.; writing—original draft preparation, K.P.-F.; writing—review and editing, K.P.-F.; supervision, K.P.-F.; funding acquisition, K.P.-F. All authors have read and agreed to the published version of the manuscript.

Funding: This research was supported by the National Science Centre of Poland (Grant No. 2018/28/T/ST10/00528).

Acknowledgments: The authors are very grateful to Tomasz Wojciechowski from Polish National Geological Institute for providing geological data and documentation from the study area.

Conflicts of Interest: The authors declare no conflict of interest.

Appendix A

Table A1. Probability Frequency Ratio Indexes Calculated for each LCFs Based on SOPO Database and Gródek Study Area.

Factors	Class	Pixels in Domain		Pixels of Landslides		FR
		No	%	No	%	
Curvature	−979.75–−37.75	291,592	0.75	29,939	0.92	1.23
	−37.75–−12.75	1,687,349	4.32	229,537	7.02	1.63
	−12.75–−1.75	10,372,349	26.55	983,957	30.10	1.13
	−1.75–6.50	22,079,144	56.51	1,460,148	44.66	0.79
	6.50–22.50	3,940,830	10.09	489,893	14.98	1.49
	22.50–1140.75	701,338	1.79	75,768	2.32	1.29
Faults Proximity [m]	0–765.01	26,053	28.99	2190	56.93	1.96
	765.01–1586.69	25,432	28.30	1387	36.05	1.27
	1586.69–2521.70	18,475	20.56	225	5.85	0.28
	2521.70–3626.72	10,900	12.13	45	1.17	0.10
	3626.72–5015.07	5775	6.43	0	0.00	0.00
	5015.07–7253.44	3223	3.59	0	0.00	0.00
Flow Direction	1–37	28,223,380	72.23	2,615,096	79.99	1.11
	37–77	6,242,526	15.98	405,102	12.39	0.78
	77–109	13,119	0.03	59	0.00	0.05
	109–157	4,572,240	11.70	248,918	7.61	0.65
	157–214	13,417	0.03	54	0.00	0.05
	214–255	7920	0.02	13	0.00	0.02
Lake Proximity [m]	0–649.33	13,232,213	33.57	901,498	27.57	0.82
	649.33–1593.82	9,813,224	24.90	1,046,185	31.99	1.29
	1593.82–2597.33	7,082,092	17.97	776,086	23.73	1.32
	2597.33–3748.42	4,586,819	11.64	378,071	11.56	0.99
	3748.42–5224.17	3,010,943	7.64	145,170	4.44	0.58
	5224.17–7555.87	1,691,373	4.29	23,073	0.71	0.16
Plan Curvature	−701.06–−45.17	24,815	0.06	2,549	0.08	1.23
	−45.17–−22.74	131,431	0.34	16,280	0.50	1.48
	−22.74–−11.53	486,180	1.24	70,428	2.15	1.73
	−11.53–−5.93	1,258,467	3.22	191,990	5.87	1.82
	−5.93–−0.32	13,687,923	35.03	1,180,094	36.10	1.03
	−0.32–734.06	23,483,786	60.10	1,807,901	55.30	0.92

Table A1. *Cont.*

Factors	Class	Pixels in Domain		Pixels of Landslides		FR
		No	%	No	%	
Precipitations [mm/yr]	696.41–730.70	4,812	7.70	1,126	21.15	2.75
	730.70–756.92	6,353	10.17	467	8.77	0.86
	756.92–780.64	7,722	12.36	721	13.54	1.10
	780.64–801.77	9,823	15.72	287	5.39	0.34
	801.77–820.00	12,792	20.47	995	18.69	0.91
	820.00–845.59	20,995	33.59	1,729	32.47	0.97
Profile Curvature	−586.48–−33.85	57,049	0.15	4,023	0.12	0.84
	−33.85–−15.11	680,793	1.74	67,693	2.07	1.19
	−15.11–−5.75	2,364,978	6.05	297,630	9.10	1.50
	−5.75–3.62	31,249,522	79.98	2,312,749	70.74	0.88
	3.62–22.35	4,339,699	11.11	552,646	16.90	1.52
	22.35–612.45	380,561	0.97	34,501	1.06	1.08
Roads Proximity [m]	0–55.03	14,884,008	37.76	1,075,148	32.88	0.87
	55.03–119.36	10,966,840	27.82	986,543	30.17	1.08
	119.36–200.64	7,044,541	17.87	701,848	21.46	1.20
	200.64–310.73	3,746,656	9.51	389,038	11.90	1.25
	310.73–461.87	1,920,345	4.87	97,124	2.97	0.61
	461.87–783.52	854,274	2.17	20,382	0.62	0.29
SEI	−71.26–−17.39	2,171,892	5.56	282,035	8.62	1.55
	−17.39–−6.15	7,539,677	19.30	671,358	20.53	1.06
	−6.15–2.13	15,204,875	38.93	742,829	22.72	0.58
	2.13–9.24	7,830,238	20.05	831,721	25.43	1.27
	9.24–19.89	5,081,182	13.01	604,915	18.50	1.42
	19.89–79.67	1,228,866	3.15	137,189	4.20	1.33
Slope [°]	0–4.46	9,736,000	24.93	179,319	5.49	0.22
	4.46–10.50	11,099,321	28.43	935,294	28.61	1.01
	10.50–16.55	9,289,000	23.79	1,011,335	30.93	1.30
	16.55–23.87	5,062,145	12.96	660,112	20.19	1.56
	23.87–33.73	2,788,488	7.14	366,922	11.22	1.57
	33.73–81.46	1,072,347	2.75	116,260	3.56	1.29
Streams Proximity [m]	0–59.67	13,517,570	34.42	1,480,964	45.29	1.32
	59.67–127.28	10,430,942	26.56	1,057,532	32.34	1.22
	127.28–206.81	7,694,317	19.59	529,470	16.19	0.83
	206.81–310.66	4,816,996	12.27	163,348	5.00	0.41
	310.66–468.80	1,987,450	5.06	35,587	1.09	0.22
	468.80–821.72	824,373	2.10	2,972	0.09	0.04
Thrusts Proximity [m]	0–556.97	33,107	28.12	2,165	34.15	1.21
	556.97–1247.63	31,171	26.48	1,038	16.37	0.62
	1247.63–2027.39	22,416	19.04	569	8.98	0.47
	2027.39–2940.84	15,252	12.96	755	11.91	0.92
	2940.84–3987.95	9789	8.32	984	15.52	1.87
	3987.95–5703.44	5984	5.08	828	13.06	2.57
Aspect [°]	−1–56.82	7,170,558	18.36	376,448	11.51	0.63
	56.82–118.86	5,320,000	13.62	332,974	10.19	0.75
	118.86–178.09	5,986,026	15.33	471,931	14.44	0.94
	178.09–235.91	7,716,443	19.76	746,049	22.82	1.15
	235.91–297.95	6,014,624	15.40	705,511	21.58	1.40
	297.95–360	6,839,650	17.52	636,329	19.46	1.11
CTI	0.06–4.15	7,790,441	19.95	963,676	29.47	1.48
	4.15–5.61	11,361,374	29.09	1,126,855	34.46	1.18
	5.61–7.07	9,614,984	24.62	655,065	20.03	0.81
	7.07–8.72	6,253,701	16.01	320,192	9.79	0.61
	8.72–10.86	3,030,027	7.76	154,055	4.71	0.61
	10.86–24.97	1,006,203	2.58	50,204	1.54	0.60
IMI	−24.08–226.20	37,992,784	97.28	3,146,601	96.22	0.99
	226.2–1227.34	907,663	2.32	102,964	3.15	1.35
	1227.34–3354.77	118,145	0.30	16,996	0.52	1.72
	3354.77–7109.06	29,122	0.07	3225	0.10	1.32
	7109.056–14,742.77	6782	0.02	230	0.01	0.41
	14,742.77–32,012.48	1004	0.00	31	0.00	0.37

Table A1. *Cont.*

Factors	Class	Pixels in Domain		Pixels of Landslides		FR
		No	%	No	%	
NDVI	−0.55–−0.11	15,232	3.90	0	0.00	0.00
	−0.11–0.12	13,774	3.53	110	0.33	0.09
	0.12–0.35	36,583	9.37	1154	3.51	0.37
	0.35–0.52	49,905	12.78	2473	7.53	0.59
	0.52–0.65	124,683	31.93	9729	29.61	0.93
	0.65–0.85	150,351	38.50	19,388	59.01	1.53
Elevation [m]	232.83–285.05	10,648,847	27.25	224,023	6.85	0.25
	285.05–329.55	6,956,591	17.80	983,068	30.07	1.69
	329.55–374.20	6,966,168	17.83	879,834	26.91	1.51
	374.20–421.18	6,642,407	17.00	668,929	20.46	1.20
	421.18–475.72	5,164,608	13.22	416,263	12.73	0.96
	475.72–613.87	2,693,981	6.89	97,125	2.97	0.43
Land Cover	Forest	613,416	35.52	72,349	55.25	1.56
	Water	122,254	7.08	26	0.02	0.00
	Buildings	342,929	19.86	22,149	16.91	0.85
	Bare earth (agriculture)	165,758	9.60	6456	4.93	0.51
	Agricultural Areas	482,418	27.94	29,965	22.88	0.82
Tectonics	1—Quaternary Units	15,545	20.52	27.00	0.42	0.02
	2—Silesian Nappe (Tertiary period—Paleocene)	27,017	35.66	2969	45.97	1.29
	3—Silesian Nappe (Upper Cretaceous)	14,342	18.93	854	13.22	0.70
	4—Silesian Nappe (Lower Cretaceous)	482	0.64	0	0.00	0.00
	5—Under Magura Nappe Dukielskie series (Tertiary period—Palaeogene)	1827	2.41	53	0.82	0.34
	6—Grybów and Michalczowej Unit (Tertiary period—Palaeogene)	9316	12.30	930	14.40	1.17
	7—Magura Nappe (Tertiary period—Palaeogene)	7241	9.56	1625	25.16	2.63
Lithostratigraphic unit	3—gravel, sands and clays, ore dregs of the valley bottoms (Quaternary)	8162	10.76	18	0.28	0.03
	4—clay, slıts with admixture pf sands and alluvial soils, river sands and gasses of flooding and overflow terraces 1–5 m on the riverbank (Quaternary)	3585	4.73	0	0.00	0.00
	5—rock rubbles in situ (Quaternary)	53	0.07	0	0.00	0.00
	6—sands and weathering clays (Quaternary)	371	0.49	4	0.06	0.13
	7—clays, sands, clays, sometimes with congregational and diluvial rubble (Quaternary)	277	0.37	0	0.00	0.00
	9—loess-like clays (Quaternary)	139	0.18	0	0.00	0.00
	10—gravel, sands and river clays, erosive and storage terraces 6–13 m on the riverbank (Quaternary)	2634	3.47	5	0.08	0.02
	11—gravel, sands and river clays, erosive and storage terraces 15–30 m on the riverbank (Quaternary)	228	0.30	0	0.00	0.00
	12—boulders, gravel and water type sand (Quaternary)	96	0.13	0	0.00	0.00

Table A1. *Cont.*

Factors	Class	Pixels in Domain		Pixels of Landslides		FR
		No	%	No	%	
	22—shale and sandstones (Tertiary period—Paleocene)	1771	2.34	54	0.84	0.36
	23—darkish limestone(Tertiary period—Paleocene)	21	0.03	0	0.00	0.00
	24—medium-thick and semi-thin sandstone and shale (Tertiary period—Paleocene)	12,740	16.80	457	7.08	0.42
	25—shale, sandstone, chert, marl, and conglomerate-menilite layers (Tertiary period—Paleocene)	675	0.89	90	1.39	1.57
	26—globigerina marl (Tertiary period—Paleocene)	85	0.11	38	0.59	5.25
	27—sandstone and shale–hieroglyph layers (Tertiary period—Paleocene)	3029	3.99	1096	16.97	4.25
	28—sandstone and shale—heavy type sandstone (Tertiary period—Paleocene)	2871	3.79	517	8.01	2.11
	29—shale with thick-bedded and medium-bedded sandstone inserts (Tertiary period—Paleocene)	637	0.84	106	1.64	1.95
	30—sandstone and conglomerate—upper Istebna sandstone (Tertiary period—Paleocene)	1308	1.72	111	1.72	1.00
	31—shale with thin-bedded sandstone inserts (Tertiary period—Paleocene)	2430	3.20	309	4.78	1.49
	32—Istebna shale with lower layers from upper Istebna (Upper Cretaceous)	1510	1.99	191	2.96	1.49
	33—sandstone and conglomerate—lower Istebna layers (Upper Cretaceous)	11,383	15.01	630	9.76	0.65
	34—thin, thick and medium-bedded sandstone, seated conglomerate—unseparated Godulskie layers (Upper Cretaceous)	2959	3.90	224	3.47	0.89
	39—Rzewów shales (Lower Cretaceous)	58	0.08	0	0.00	0.00
	40—sandstone-Grodziskie layers (Lower Cretaceous)	119	0.16	0	0.00	0.00
	41—shale with thin-bedded sandstone inserts—upper Cieszyn shales (Lower Cretaceous)	305	0.40	0	0.00	0.00
	42—thick-bedded sandstone—Cergowa sandstone (Tertiary period—Palaeogene)	1406	1.85	53	0.82	0.44
	43—shales menilite and lower Cergowa mar (Tertiary period—Palaeogene)	341	0.45	0	0.00	0.00
	44—shales or shale and sandstone—hieroglyphs and green shale (Tertiary period—Palaeogene)	80	0.11	0	0.00	0.00

Table A1. *Cont.*

Factors	Class	Pixels in Domain		Pixels of Landslides		FR
		No	%	No	%	
	45—tylawskie limestone (Tertiary period—Palaeogene)	4650	6.13	490	7.59	1.24
	46—Sandstone and shale (Tertiary period—Palaeogene)	51	0.07	0	0.00	0.00
	47—Shale, chert, sandstone—Grybowskie layers (Tertiary period—Palaeogene)	3468	4.57	205	3.17	0.69
	48—Organodetic limestone and sandstone—Luzańskie lımestone and Michalczowej sandstone (Tertiary period—Palaeogene)	325	0.43	36	0.56	1.30
	49—marn shale, sandstone, lower Grybowskıe marl (Tertiary period—Palaeogene)	284	0.37	0	0.00	0.00
	50—shale and sandstone–hieroglyph layers (Tertiary period—Palaeogene)	391	0.52	199	3.08	5.98
	51—spotted shale (Tertiary period—Palaeogene)	147	0.19	0	0.00	0.00
	52—thin and medium-bedded sandstones and shales—layers of Jawoveret/inoceramic in biotite facies (Tertiary period—Palaeogene)	60	0.08	0	0.00	0.00
	53—sandstone and shale-Magura layers in glauconite faction (Tertiary period—Palaeogene)	151	0.20	0	0.00	0.00
	56—chert, Pelic limestone (Tertiary period—Palaeogene)	562	0.74	0	0.00	0.00
	59—Ciężkowice sandstones in the Magura sandstone form of Wojakowa (Tertiary period—Palaeogene)	835	1.10	0	0.00	0.00
	60—spotted shale (Tertiary period—Palaeogene)	779	1.03	8	0.12	0.12
	62—medium and thin-bedded sandstones and shales—layers of Kanina (Tertiary period—Palaeogene)	1783	2.35	772	11.95	5.08
	63—marl and spotted shale (Tertiary period—Palaeogene)	3071	4.05	845	13.08	3.23
Soil Suitability	2—medium grassland complex	73,017	4.65	5,034	3.83	0.82
	3—grassland weak and very weak	469	0.03	171	0.13	4.35
	8—strong grain and fodder complex	69,232	4.41	4639	3.53	0.80
	10—mountains wheat complex	188,272	12.00	1078	0.82	0.07
	11—mountainous grain complex	573,446	36.54	52,866	40.20	1.10
	13—oat fodder mountainous complex	4801	0.31	483	0.37	1.20
	14—Arable soils intended for grassland	10,277	0.65	4679	3.56	5.43
	20—forest	264,201	16.83	46,219	35.14	2.09
	21—barren	9995	0.64	0	0.00	0.00
	23—forest clay sands	137,252	8.75	11,827	8.99	1.03

Table A1. *Cont.*

Factors	Class	Pixels in Domain		Pixels of Landslides		FR
		No	%	No	%	
	24—agriculturally unsuitable soils suitable for afforestation	1055	0.07	673	0.51	7.61
	25-agricultural areas	3,549	0.23	416	0.32	1.40
	26—water	215,609	13.74	1695	1.29	0.09
	33—defective wheat complex	18,236	1.16	1730	1.32	1.13

Appendix B

Table A2. Probability Frequency Ratio Indexes Calculated for each LCFs Based on SOPO Database and Łososina Study Area.

Factors	Class	Pixels in Domain		Pixels of Landslides		FR
		No	%	No	%	
Curvature	−979.75–−37.75	291,592	0.75	23,642	1.12	1.51
	−37.75–−12.75	1,687,349	4.32	168,559	8.02	1.86
	−12.75–−1.75	10,372,349	26.55	635,081	30.21	1.14
	−1.75–6.50	22,079,144	56.51	880,022	41.86	0.74
	6.50–22.50	3,940,830	10.09	334,674	15.92	1.58
	22.50–1140.75	701,338	1.79	60,341	2.87	1.60
Faults Proximity [m]	0–765.01	26,053	28.99	660	20.65	0.71
	765.01–1586.69	25,432	28.30	749	23.44	0.83
	1586.69–2521.70	18,475	20.56	1227	38.39	1.87
	2521.70–3626.72	10,900	12.13	498	15.58	1.28
	3626.72–5015.07	5775	6.43	62	1.94	0.30
	5015.07–7253.44	3223	3.59	0	0.00	0.00
Flow Direction	1–37	28,223,380	72.23	1,674,906	79.67	1.10
	37–77	6,242,526	15.98	179,941	8.56	0.54
	77–109	13,119	0.03	33	0.00	0.05
	109–157	4,572,240	11.70	247,419	11.77	1.01
	157–214	13,417	0.03	20	0.00	0.03
	214–255	7920	0.02	0	0.00	0.00
Lake Proximity [m]	0–649.33	13,232,213	33.57	1,004,964	47.79	1.42
	649.33–1593.82	9,813,224	24.90	730,394	34.73	1.40
	1593.82–2597.33	7,082,092	17.97	353,360	16.80	0.94
	2597.33–3748.42	4,586,819	11.64	14,066	0.67	0.06
	3748.42–5224.17	3,010,943	7.64	33	0.00	0.00
	5224.17–7555.87	1,691,373	4.29	0	0.00	0.00
Planar Curvature	−701.06–−45.17	24,815	0.06	2138	0.10	1.60
	−45.17–−22.74	131,431	0.34	12,925	0.61	1.83
	−22.74–−11.53	486,180	1.24	52,705	2.51	2.01
	−11.53–−5.93	1,258,467	3.22	135,593	6.45	2.00
	−5.93–−0.32	13,687,923	35.03	747,311	35.55	1.01
	−0.32–734.06	23,483,786	60.10	1,151,647	54.78	0.91
Precipitations [mm/yr]	696.41–730.70	4812	7.70	9	0.26	0.03
	730.70–756.92	6353	10.17	285	8.23	0.81
	756.92–780.64	7722	12.36	0	0.00	0.00
	780.64–801.77	9823	15.72	817	23.58	1.50
	801.77- 820.00	12,792	20.47	1427	41.18	2.01
	820.00–845.59	20,995	33.59	927	26.75	0.80
Profile Curvature	−586.48–−33.85	57,049	0.15	3716	0.18	1.21
	−33.85–−15.11	680,793	1.74	52,138	2.48	1.42
	−15.11–−5.75	2,364,978	6.05	211,106	10.04	1.66
	−5.75–3.62	31,249,522	79.98	1,417,790	67.44	0.84
	3.62–22.35	4,339,699	11.11	390,276	18.56	1.67
	22.35–612.45	380,561	0.97	27,293	1.30	1.33

Table A2. *Cont.*

Factors	Class	Pixels in Domain		Pixels of Landslides		FR
		No	%	No	%	
Roads Proximity [m]	0–55.03	14,884,008	37.76	724,844	34.47	0.91
	55.03–119.36	10,966,840	27.82	705,339	33.54	1.21
	119.36–200.64	7,044,541	17.87	461,458	21.94	1.23
	200.64–310.73	3,746,656	9.51	165,853	7.89	0.83
	310.73–461.87	1,920,345	4.87	42,200	2.01	0.41
	461.87–783.52	854,274	2.17	3123	0.15	0.07
SEI	−71.26–−17.39	2,171,892	5.56	171,763	8.17	1.47
	−17.39–−6.15	7,539,677	19.30	330,655	15.73	0.81
	−6.15–2.13	15,204,875	38.93	407,265	19.37	0.50
	2.13–9.24	7,830,238	20.05	536,617	25.52	1.27
	9.24–19.89	5,081,182	13.01	475,949	22.64	1.74
	19.89–79.67	1,228,866	3.15	180,188	8.57	2.72
Slope [°]	0.000074–4.46	9,736,000	24.93	82,122	3.91	0.16
	4.46–10.50	11,099,321	28.43	494,938	23.54	0.83
	10.50–16.55	9,289,000	23.79	582,204	27.69	1.16
	16.55–23.87	50,621,45	12.96	459,570	21.86	1.69
	23.87–33.73	2,788,488	7.14	355,980	16.93	2.37
	33.73–81.46	1,072,347	2.75	127,466	6.06	2.21
Streams Proximity [m]	0–59.67	13,517,570	34.42	942,196	44.85	1.30
	59.67–127.28	10,430,942	26.56	641,522	30.54	1.15
	127.28–206.81	7,694,317	19.59	330,290	15.72	0.80
	206.81–310.66	4,816,996	12.27	144,706	6.89	0.56
	310.66–468.80	1,987,450	5.06	41,752	1.99	0.39
	468.80–821.72	824,373	2.10	392	0.02	0.01
Thrusts Proximity [m]	0–556.97	33,107	28.12	1537	36.34	1.29
	556.97–1247.63	31,171	26.48	1306	30.88	1.17
	1247.63–2027.39	22,416	19.04	917	21.68	1.14
	2027.39–2940.84	15,252	12.96	348	8.23	0.64
	2940.84–3987.95	9789	8.32	121	2.86	0.34
	3987.95–5703.44	5984	5.08	0	0.00	0.00
Aspect [°]	−1–56.82	7,170,558	18.36	280,161	13.33	0.73
	56.82–118.86	5,320,000	13.62	458,783	21.82	1.60
	118.86–178.09	5,986,026	15.33	561,221	26.70	1.74
	178.09–235.91	7,716,443	19.76	373,687	17.78	0.90
	235.91–297.95	6,014,624	15.40	229,866	10.93	0.71
	297.95–360	6,839,650	17.52	198,562	9.45	0.54
CTI	0.06–4.15	7,790,441	19.95	669,369	31.84	1.60
	4.15–5.61	11,361,374	29.09	690,270	32.83	1.13
	5.61–7.07	9,614,984	24.62	408,081	19.41	0.79
	7.07–8.72	6,253,701	16.01	201,824	9.60	0.60
	8.72–10.86	3,030,027	7.76	97,503	4.64	0.60
	10.86–24.97	1,006,203	2.58	35,390	1.68	0.65
IMI	−24.08–226.20	37,992,784	97.28	2,014,350	95.81	0.98
	226.2–1227.34	907,663	2.32	69,553	3.31	1.42
	1227.34–3354.77	118,145	0.30	13,966	0.66	2.20
	3354.77–7109.06	29,122	0.07	3761	0.18	2.40
	7109.056–14,742.77	6782	0.02	717	0.03	1.96
	14,742.77–32,012.48	1004	0.00	72	0.00	1.33
NDVI	−0.55–−0.11	15,232	3.90	0	0.00	0.00
	−0.11–0.12	13,774	3.53	0	0.00	0.00
	0.12–0.35	36,583	9.37	474	2.25	0.24
	0.35–0.52	49,905	12.78	1297	6.16	0.48
	0.52–0.65	124,683	31.93	5938	28.21	0.88
	0.65–0.85	150,351	38.50	13,342	63.38	1.65
Elevation [m]	232.83–285.05	10,648,847	27.25	433,742	20.63	0.76
	285.05–329.55	6,956,591	17.80	862,559	41.03	2.30
	329.55–374.20	6,966,168	17.83	528,893	25.16	1.41
	374.20–421.18	6,642,407	17.00	164,675	7.83	0.46
	421.18–475.72	5,164,608	13.22	66,068	3.14	0.24
	475.72–613.87	2,693,981	6.89	46,382	2.21	0.32

Table A2. *Cont.*

Factors	Class	Pixels in Domain		Pixels of Landslides		FR
		No	%	No	%	
Land Cover	Forest	613,416	35.52	72,349	55.25	1.56
	Water	122,254	7.08	26	0.02	0.00
	Buildings	342,929	19.86	22,149	16.91	0.85
	Bare earth (agriculture)	165,758	9.60	6456	4.93	0.51
	Agricultural Areas	482,418	27.94	29,965	22.88	0.82
Tectonics	1—Quaternary Units	15,545	20.52	27.00	0.42	0.02
	2—Silesian Nappe (Tertiary period—Paleocene)	27,017	35.66	2,969	45.97	1.29
	3—Silesian Nappe (Upper Cretaceous)	14,342	18.93	854	13.22	0.70
	4—Silesian Nappe (Lower Cretaceous)	482	0.64	0	0.00	0.00
	5—Under Magura Nappe Dukielskie series (Tertiary period—Palaeogene)	1827	2.41	53	0.82	0.34
	6—Grybów and Michalczowej Unit (Tertiary period—Palaeogene)	9316	12.30	930	14.40	1.17
	7—Magura Nappe (Tertiary period—Palaeogene)	7241	9.56	1625	25.16	2.63
Lithostratigraphic unit	3—gravel, sands and clays, ore dregs of the valley bottoms (Quaternary)	8162	10.76	18	0.28	0.03
	4—clay, slıts with admixture pf sands and alluvial soils, river sands and gasses of flooding and overflow terraces 1–5 m on the riverbank (Quaternary)	3585	4.73	0	0.00	0.00
	5—rock rubbles in situ(Quaternary)	53	0.07	0	0.00	0.00
	6—sands and weathering clays(Quaternary)	371	0.49	4	0.06	0.13
	7—clays, sands, clays, sometimes with congregational and diluvial rubble (Quaternary)	277	0.37	0	0.00	0.00
	9—loess-like clays(Quaternary)	139	0.18	0	0.00	0.00
	10—gravel, sands and river clays, erosive and storage terraces 6–13 m on the riverbank (Quaternary)	2634	3.47	5	0.08	0.02
	11—gravel, sands and river clays, erosive and storage terraces. 15–30 m (Quaternary)on the riverbank (Quaternary)	228	0.30	0	0.00	0.00
	12—boulders, gravel and water type sand (Quaternary)	96	0.13	0	0.00	0.00
	22—shale and sandstones (Tertiary period—Paleocene)	1771	2.34	54	0.84	0.36
	23—darkish limestone (Tertiary period—Paleocene)	21	0.03	0	0.00	0.00
	24—medium-thick and semi-thin sandstone and shale (Tertiary period—Paleocene)	12,740	16.80	457	7.08	0.42
	25—shale, sandstone, chert, marl, and conglomerate-menilite layers (Tertiary period—Paleocene)	675	0.89	90	1.39	1.57
	26—globigerina marl (Tertiary period—Paleocene)	85	0.11	38	0.59	5.25

Table A2. *Cont.*

Factors	Class	Pixels in Domain		Pixels of Landslides		FR
		No	%	No	%	
	27—sandstone and shale–hieroglyph layers (Tertiary period—Paleocene)	3029	3.99	1096	16.97	4.25
	28—sandstone and shale—heavy type sandstone (Tertiary period—Paleocene)	2871	3.79	517	8.01	2.11
	29—shale with thick-bedded and medium-bedded sandstone inserts (Tertiary period—Paleocene)	637	0.84	106	1.64	1.95
	30—sandstone and conglomerate—upper Istebna sandstone (Tertiary period—Paleocene)	1308	1.72	111	1.72	1.00
	31—shale with thin-bedded sandstone inserts (Tertiary period—Paleocene)	2430	3.20	309	4.78	1.49
	32—Istebna shale with lower layers from upper Istebna (Upper Cretaceous)	1510	1.99	191	2.96	1.49
	33—sandstone and conglomerate—lower Istebna layers (Upper Cretaceous)	11,383	15.01	630	9.76	0.65
	34—thin, thick and medium-bedded sandstone, seated conglomerate—unseparated Godulskie layers (Upper Cretaceous)	2959	3.90	224	3.47	0.89
	39—Rzewów shales (Lower Cretaceous)	58	0.08	0	0.00	0.00
	40—sandstone-Grodziskie layers (Lower Cretaceous)	119	0.16	0	0.00	0.00
	41—shale with thin-bedded sandstone inserts—upper Cieszyn shales (Lower Cretaceous)	305	0.40	0	0.00	0.00
	42—thick-bedded sandstone—Cergowa sandstone (Tertiary period—Palaeogene)	1406	1.85	53	0.82	0.44
	43—shales menilite and lower Cergowa mar (Tertiary period—Palaeogene)	341	0.45	0	0.00	0.00
	44—shales or shale and sandstone—hieroglyphs and green shale (Tertiary period—Palaeogene)	80	0.11	0	0.00	0.00
	45—tylawskie limestone (Tertiary period—Palaeogene)	4650	6.13	490	7.59	1.24
	46—Sandstone and shale (Tertiary period—Palaeogene)	51	0.07	0	0.00	0.00
	47—Shale, chert, sandstone—Grybowskie layers (Tertiary period—Palaeogene)	3468	4.57	205	3.17	0.69
	48—Organodetic limestone and sandstone—Luzańskie lımestone and Michalczowej sandstone (Tertiary period—Palaeogene)	325	0.43	36	0.56	1.30
	49—marn shale, sandstone, lower Grybowskıe marl (Tertiary period—Palaeogene)	284	0.37	0	0.00	0.00

Table A2. *Cont.*

Factors	Class	Pixels in Domain No	Pixels in Domain %	Pixels of Landslides No	Pixels of Landslides %	FR
	50—shale and sandstone–hieroglyph layers (Tertiary period—Palaeogene)	391	0.52	199	3.08	5.98
	51—spotted shale (Tertiary period—Palaeogene)	147	0.19	0	0.00	0.00
	52—thin and medium-bedded sandstones and shales—layers of Jawoveret/inoceramic in biotite facies (Tertiary period—Palaeogene)	60	0.08	0	0.00	0.00
	53—sandstone and shale-Magura layers in glauconite faction (Tertiary period—Palaeogene)	151	0.20	0	0.00	0.00
	56—chert, Pelic limestone (Tertiary period—Palaeogene)	562	0.74	0	0.00	0.00
	59—Ciężkowice sandstones in the Magura sandstone form of Wojakowa (Tertiary period—Palaeogene)	835	1.10	0	0.00	0.00
	60—spotted shale (Tertiary period—Palaeogene)	779	1.03	8	0.12	0.12
	62—medium and thin-bedded sandstones and shales—layers of Kanina (Tertiary period—Palaeogene)	1783	2.35	772	11.95	5.08
	63—marl and spotted shale (Tertiary period—Palaeogene)	3071	4.05	845	13.08	3.23
Soil suitability	2—medium grassland complex	73,017	4.65	7861	9.29	2.00
	3—grassland weak and very weak	469	0.03	0	0.00	0.00
	8—strong grain and fodder complex	69,232	4.41	4494	5.31	1.20
	10—mountains wheat complex	188,272	12.00	3672	4.34	0.36
	11—mountainous grain complex	573,446	36.54	28,503	33.68	0.92
	13—oat fodder mountainous complex	4801	0.31	134	0.16	0.52
	14—Arable soils intended for grassland	10,277	0.65	1328	1.57	2.40
	20—forest	264,201	16.83	21,568	25.49	1.51
	21—barren	9995	0.64	96	0.11	0.18
	23—forest clay sands	137,252	8.75	12,645	14.94	1.71
	24—agriculturally unsuitable soils suitable for afforestation	1055	0.07	0	0.00	0.00
	25—agricultural areas	3549	0.23	0	0.00	0.00
	26—water	215,609	13.74	1099	1.30	0.09
	33—defective wheat complex	18,236	1.16	3223	3.81	3.28

References

1. Cruden, D.M.; Varnes, D.J. Landslide types and processes. In *Landslides: Investigation and Mitigation*; Turner, A.K., Schuster, R.L., Eds.; Transportation Research Board: Washington, DC, USA, 1996.
2. Lin, L.; Lin, Q.; Wang, Y. Landslide susceptibility mapping on a global scale using the method of logistic regression. *Nat. Hazards Earth Syst. Sci.* **2017**, *18*, 1411–1424. [CrossRef]

3. Arabameri, A.; Pradhan, B.; Rezaei, K.; Sohrabi, M.; Kalantari, Z. GIS-based landslide susceptibility mapping using numerical risk factor bivariate model and its ensemble with linear multivariate regression and boosted regression tree algorithms. *J. Mt. Sci.* **2019**, *16*, 595–618. [CrossRef]
4. Nicodemo, G.; Peduto, D.; Ferlisi, S.; Gullà, G.; Borrelli, L.; Fornaro, G.; Reale, D. Analysis of building vulnerability to slow-moving landslides via A-DInSAR and damage survey data. In *Advancing Culture of Living with Landslides*; Mikos, M., Tiwari, Y., Sassa, Y., Eds.; Springer: Cham, Switzerland, 2017; pp. 889–907. [CrossRef]
5. Borrelli, L.; Nicodemo, G.; Ferlisi, S.; Peduto, D.; Di Nocera, S.; Gullà, G. Geology, slow-moving landslides, and damages to buildings in the Verbicaro area (North-Western Calabria Region, Southern Italy). *J. Maps* **2018**, *14*, 32–44. [CrossRef]
6. Nadim, F.; Kjekstad, O.; Peduzzi, P.; Herold, C.; Jaedicke, C. Global landslide and avalanche hotspots. *Landslides* **2006**, *3*, 159–173. [CrossRef]
7. Poprawa, D.; Rączkowski, W. Osuwiska Karpat. *Przegląd Geol.* **2014**, *51*, 685–692. (In Polish)
8. Borkowski, A.; Perski, Z.; Wojciechowski, T.; Józków, G.; Wójcik, A. Landslides mapping in Roznów Lake vicinity, Poland using airborne laser scanning data. *Acta Geodynamica Geomater.* **2011**, *8*, 325–333.
9. Wojciechowski, T.; Borkowski, A.; Perski, Z.; Wójcik, A. Airborne laser scanning data in landslide studies at the example of the Zbyszyce landslide (Outer Carpathians). *Przegląd Geol.* **2012**, *60*, 95–102. (In Polish)
10. Cascini, L.; Ciurleo, M.; Di Nocera, S.; Gullà, G. A new–old approach for shallow landslide analysis and susceptibility zoning in fine-grained weathered soils of southern Italy. *Geomorphology* **2015**, *241*, 371–381. [CrossRef]
11. Ciurleo, M.; Mandaglio, M.C.; Moraci, N. Landslide susceptibility assessment by TRIGRS in a frequently affected shallow instability area. *Landslides* **2019**, *16*, 175–188. [CrossRef]
12. Guzzetti, F. Landslide Hazard and Risk Assessment. Ph.D. Thesis, Mathematisch-Naturwissenschaftlichen Fakultät der Rheinischen Friedrich-Wilhelms-University of Bonn, Bonn, Germany, 2006.
13. Arabameri, A.; Saha, S.; Roy, J.; Chen, W.; Blaschke, T.; Tien Bui, D. Landslide susceptibility evaluation and management using different machine learning methods in the Gallicash River Watershed, Iran. *Remote Sens.* **2020**, *12*, 475. [CrossRef]
14. Pawluszek, K.; Borkowski, A. Impact of DEM-derived factors and analytical hierarchy process on landslide susceptibility mapping in the region of Rożnów Lake, Poland. *Nat. Hazards* **2017**, *86*, 919–952. [CrossRef]
15. Paudel, U.; Oguchi, T.; Hayakawa, Y. Multi-resolution landslide susceptibility analysis using a DEM and random forest. *Int. J. Geosci.* **2016**, *7*, 726–743. [CrossRef]
16. Saadatkhah, N.; Kassim, A.; Lee, L.M. Qualitative and quantitative landslide susceptibility assessments in Hulu Kelang area, Malaysia. *Electron. J. Geotech. Eng.* **2014**, *19*, 545–563.
17. Ciurleo, M.; Mandaglio, M.C.; Moraci, N.; Pitasi, A. A method to evaluate debris flow triggering and propagation by numerical analyses. In *Geotechnical Research for Land Protection and Development. CNRIG 2019. Lecture Notes in Civil Engineering*; Calvetti, F., Cotecchia, F., Galli, A., Jommi, C., Eds.; Springer: Cham, Switzerland, 2019; Volume 40, pp. 33–41.
18. Chen, W.; Xie, X.; Peng, J.; Shahabi, H.; Hong, H.; Bui, D.T.; Zhu, A.X. GIS-based landslide susceptibility evaluation using a novel hybrid integration approach of bivariate statistical based random forest method. *Catena* **2018**, *164*, 135–149. [CrossRef]
19. Aditian, A.; Kubota, T.; Shinohara, Y. Comparison of GIS-based landslide susceptibility models using frequency ratio, logistic regression, and artificial neural network in a tertiary region of Ambon, Indonesia. *Geomorphology* **2018**, *318*, 101–111. [CrossRef]
20. Razavizadeh, S.; Solaimani, K.; Massironi, M.; Kavian, A. Mapping landslide susceptibility with frequency ratio, statistical index, and weights of evidence models: A case study in northern Iran. *Environ. Earth Sci.* **2017**, *76*, 499. [CrossRef]
21. Lee, S.; Oh, H.J. Landslide susceptibility prediction using evidential belief function, weight of evidence and artificial neural network models. *Korean J. Remote Sens.* **2019**, *35*, 299–316.
22. Shirani, K.; Pasandi, M.; Arabameri, A. Landslide susceptibility assessment by dempster–shafer and index of entropy models, Sarkhoun basin, southwestern Iran. *Nat. Hazards* **2018**, *93*, 1379–1418. [CrossRef]
23. Kanungo, D.P.; Arora, M.K.; Sarkar, S.; Gupta, R.P. A comparative study of conventional, ANN black box, fuzzy and combined neural and fuzzy weighting procedures for landslide susceptibility zonation in Darjeeling Himalayas. *Eng. Geol.* **2006**, *85*, 347–366. [CrossRef]

24. Chen, W.; Pourghasemi, H.R.; Naghibi, S.A. A comparative study of landslide susceptibility maps produced using support vector machine with different kernel functions and entropy data mining models in China. *Bull. Eng. Geol. Environ.* **2018**, *77*, 647–664. [CrossRef]
25. Huang, Y.; Zhao, L. Review on landslide susceptibility mapping using support vector machines. *Catena* **2018**, *165*, 529. [CrossRef]
26. Zhang, K.; Wu, X.; Niu, R.; Yang, K.; Zhao, L. The assessment of landslide susceptibility mapping using random forest and decision tree methods in the Three Gorges Reservoir area, China. *Environ. Earth Sci.* **2018**, *76*, 1–20. [CrossRef]
27. Gudiyangada Nachappa, T.; Kienberger, S.; Meena, S.R.; Hölbling, D.; Blaschke, T. Comparison and validation of per-pixel and object-based approaches for landslide susceptibility mapping. *Geomat. Nat. Hazards Risk* **2020**, *11*, 572–600.
28. Javier, D.N.; Kumar, L. Frequency ratio landslide susceptibility estimation in a tropical mountain region. *Int. Arch. Photogramm. Remote Sens. Spat. Inf. Sci.* **2019**, *42*, 173–179. [CrossRef]
29. Van Den Eeckhaut, M.; Hervás, J. State of the art of national landslide databases in Europe and their potential for assessing landslide susceptibility, hazard and risk. *Geomorphology* **2012**, *139*. [CrossRef]
30. Cieszkowski, M.; Waśkowska, A. Castles from the Rożnowskie and Czchowskie lakes as geotouristic lapidaria and the role of the Istebna sandstones in their formation. *Geoturystyka* **2010**, *21*, 3–18. (In Polish)
31. Hungr, O.; Leroueil, S.; Picarelli, L. The Varnes classification of landslide types, an update. *Landslides* **2014**, *11*, 167–194. [CrossRef]
32. Dai, F.C.; Xu, C.; Yao, X.; Xu, L.; Tu, X.B.; Gong, Q.M. Spatial distribution of landslides triggered by the 2008 Ms 8.0 Wenchuan earthquake, China. *J. Asian Earth Sci.* **2011**, *40*, 883–895. [CrossRef]
33. Dou, J.; Paudel, U.; Oguchi, T.; Uchiyama, S.; Hayakavva, Y.S. Shallow and deep-seated landslide differentiation using support vector machines: A case study of the Chuetsu Area, Japan. *Terr. Atmos. Ocean. Sci.* **2015**, *26*, 227–239. [CrossRef]
34. Roering, J.J.; Schmidt, K.M.; Stock, J.D.; Dietrich, W.E.; Montgomery, D.R. Shallow landsliding, root reinforcement, and the spatial distribution of trees in the Oregon Coast Range. *Can. Geotech. J.* **2003**, *40*, 237–253. [CrossRef]
35. Bąk, M.; Długosz, M.; Gorczyca, E.; Kasina, Kozioł, T.; Wrońska-Wałach, D.; Wyderski, P. *Map of Landslides and Areas Threatened by Mass Movements on a Scale of 1: 10000 Łososina Dolna Commune, Nowosądeckie County, Małpolskie Municipality*; Ministerstwo Środowiska: Warszawa, Poland, 2011. (In Polish)
36. Wójcik, A.; Wojciechowski, T.; Wódka, M.; Krzysiek, U. *Map of Landslides and Areas Threatened by Mass Movements on a Scale of 1: 10000 Gróek nad Dunajcem Commune, Nowosądeckie County, Małpolskie Municipality*; Ministerstwo Środowiska: Warszawa, Poland, 2015. (In Polish)
37. Gorczyca, E.; Wrońska-Wałach, D. *Explanations to the Landslides Inventory Maps and Areas Prone to Mass Movements in the Scale of 1:10000. Municipality of Łososina Dolna, District: Nowosądecki, Province: Małopolskie*; Ministerstwo Środowiska: Warszawa, Poland, 2011. (In Polish)
38. Wójcik, A.; Wojciechowski, T.; Wódka, M.; Krzysiek, U. *Explanations for the Map of Landslides and Areas Threatened by Mass Movements on a Scale of 1: 10000 Gródek nad Dunajcem Commune, Nowosądeckie County, Małpolskie Manucipality*; Ministerstwo Środowiska: Warszawa, Poland, 2015. (In Polish)
39. Grabowski, D.; Marciniec, P.; Mrozek, T.; Nescieruk, P.; Rączkowski, W.; Wójcik, A.; Zimnal, Z. *Manual for Mapping Landslides and Areas Threatened by Mass Movements*; Ministerstwo Środowiska: Warszawa, Poland, 2008. (In Polish)
40. Gorczyca, E.; Wrońska-Wałach, D.; Długosz, M. Landslide Hazards in the Polish Flysch Carpathians: Example of Łososina Dolna Commune. In *Geomorphological Impacts of Extreme Weather*; Springer: Dordrecht, The Netherlands, 2013; pp. 237–250. [CrossRef]
41. Pawłuszek, K.; Ziaja, M.; Borkowski, A. Accuracy assessment of the height component of the airborne laser scanning data collected in the ISOK system for the Widawa River Valley. *Acta Sci. Polonorum. Geod. Descr. Terrarum* **2014**, *13*, 27–37.
42. Prakash, N.; Manconi, A.; Loew, S. Mapping landslides on EO data: Performance of deep learning models vs. traditional machine learning models. *Remote Sens.* **2020**, *12*, 346. [CrossRef]
43. Pawłuszek, K.; Marczak, S.; Borkowski, A.; Tarolli, P. Multi-aspect analysis of object-oriented landslide detection based on an extended set of LiDAR-derived terrain features. *ISPRS Int. J. Geo-Inf.* **2019**, *8*, 321. [CrossRef]

44. Pawluszek, K.; Borkowski, A.; Tarolli, P. Sensitivity analysis of automatic landslide mapping: Numerical experiments towards the best solution. *Landslides* **2018**, *15*, 1851–1865. [CrossRef]
45. Pawłuszek, K.; Borkowski, A.; Tarolli, P. Towards the optimal pixel size of DEM for automatic mapping of landslide areas. *Int. Arch. Photogramm. Remote Sens. Spat. Inf. Sci.* **2017**, *42*, 83–89. [CrossRef]
46. Pawłuszek, K.; Borkowski, A. Landslides identification using airborne laser scanning data derived topographic terrain attributes and support vector machine classification. *Int. Arch. Photogramm. Remote Sens. Spat. Inf. Sci.* **2017**, *8*. [CrossRef]
47. Evans, J.S.; Oakleaf, J.; Cushman, S.A.; Theobald, D. An ArcGIS Toolbox for Surface Gradient and Geomorphometric Modeling, Version 2.0-0. Available online: http://evansmurphy.wix.com/evansspatial (accessed on 3 August 2020).
48. Ozdemir, A. Landslide susceptibility mapping of vicinity of Yaka Landslide (Gelendost, Turkey) using conditional probability approach in GIS. *Environ. Geol.* **2009**, *57*, 1675–1686. [CrossRef]
49. Sharma, A.; Sur, U.; Singh, P.; Rai, P.K.; Srivastava, P.K. Probabilistic landslide hazard assessment using Statistical Information Value (SIV) and GIS Techniques: A case study of Himachal Pradesh, India. In *Techniques for Disaster Risk Management and Mitigation*; John Wiley and Sons: Hoboken, NJ, USA, 2020; pp. 197–208.
50. Pokharel, B.; Thapa, P.B. Landslide susceptibility in Rasuwa District of central Nepal after the 2015 Gorkha Earthquake. *J. Nepal Geol. Soc.* **2019**, *59*, 79–88. [CrossRef]
51. Chen, W.; Sun, Z.; Han, J. Landslide susceptibility modeling using integrated ensemble weights of evidence with logistic regression and random forest models. *Appl. Sci.* **2019**, *9*, 171. [CrossRef]
52. Pawluszek, K. Landslide features identification and morphology investigation using high-resolution DEM derivatives. *Nat. Hazards* **2019**, *96*, 311–330. [CrossRef]
53. Ahmed, B.; Rahman, M.S.; Sammonds, P.; Islam, R.; Uddin, K. Application of geospatial technologies in developing a dynamic landslide early warning system in a humanitarian context: The Rohingya refugee crisis in Cox's Bazar, Bangladesh. *Geomat. Nat. Hazards Risk* **2020**, *11*. [CrossRef]
54. Ramachandra, T.V.; Kumar, U.; Aithal, B.H.; Diwakar, P.G.; Joshi, N.V. Landslide susceptible locations in Western Ghats: Prediction through OpenModeller. In Proceedings of the 26th Annual In-House Symposium on Space Science and Technology, Bangalore, India, 28–29 January 2010; pp. 65–74.
55. Abedini, M.; Ghasemyan, B.; Mogaddam, M.R. Landslide susceptibility mapping in Bijar city, Kurdistan Province, Iran: A comparative study by logistic regression and AHP models. *Environ. Earth Sci.* **2017**, *76*, 308. [CrossRef]
56. Jenks, G.F. The data model concept in statistical mapping. *Int. Yearb. Cartogr.* **1967**, *7*, 186–190.
57. Guzzetti, F.; Reichenbach, P.; Ardizzone, F.; Cardinali, M.; Galli, M. Estimating the quality of landslide susceptibility models. *Geomorphology* **2006**, *81*, 166–184. [CrossRef]
58. Van Den Eeckhaut, M.; Hervás, J.; Jaedicke, C.; Malet, J.P.; Montanarella, L.; Nadim, F. Statistical modelling of Europe-wide landslide susceptibility using limited landslide inventory data. *Landslides* **2012**, *8*, 357–369. [CrossRef]
59. Armstrong, M.P.; Xiao, N.; Bennett, D.A. Using genetic algorithms to create multicriteria class intervals for choropleth maps. *Ann. Assoc. Am. Geogr* **2003**, *93*, 595–623. [CrossRef]
60. Cantarino, I.; Carrion, M.A.; Goerlich, F.; Ibañez, V.M. A ROC analysis-based classification method for landslide susceptibility maps. *Landslides* **2019**, *16*, 265–282. [CrossRef]
61. Baeza, C.; Lantada, N.; Amorim, S. Statistical and spatial analysis of landslide susceptibility maps with different classification systems. *Environ. Earth Sci.* **2016**, *75*. [CrossRef]
62. Süzen, M.L.; Doyuran, V. A comparison of the GIS based landslide susceptibility assessment methods: Multivariate versus bivariate. *Environ. Geol.* **2004**, *45*, 665–679. [CrossRef]
63. Gupta, R.P.; Kanungo, D.P.; Arora, M.K.; Sarkar, S. Approaches for comparative evaluation of raster GIS-based landslide susceptibility zonation maps. *Int. J. Appl. Earth Obs. Geoinf.* **2008**, *10*, 330–341. [CrossRef]
64. Mezaal, M.R.; Pradhan, B. An improved algorithm for identifying shallow and deep-seated landslides in dense tropical forest from airborne laser scanning data. *Catena* **2018**, *167*, 147–159. [CrossRef]